TRANSMITTAL MEMO

TO: Defense Technical Information Center

FROM: Nicole M. Corali, Lehigh University

DATE: December 6, 2016

SUBJECT: Final Technical Report: N00014-12-1-0023

1. ☐ Enclosed please find original(s) of the document referenced above. Please have the/both copy(s) signed by the appropriate institutional official and return fully executed document(s) to:

   Office of Research and Sponsored Programs
   Lehigh University
   526 Brodhead Avenue, 23B
   Bethlehem, PA 18015-3046

2. ☐ Please have the appropriate institutional official initial revision(s) and return to our office.

3. ☒ Enclosed please find 1 copy of the document referenced above.

Please do not hesitate to contact Nicole M. Corali, Contract and Grant Specialist at (610) 758-4585 if you have any questions or concerns.

Enclosure

cc: LU#542630

REPORT DOCUMENTATION PAGE

Form Approved
OMB No. 0704-0188

1. REPORT DATE *(DD-MM-YYYY)*	2. REPORT TYPE	3. DATES COVERED *(From - To)*
06-12-2016	Final Technical	Dec 2011 - Sept 2016

4. TITLE AND SUBTITLE
Integrating SHM and Time-Variant System Performance of Naval Ship Structures For Near Real-Time Decision Making Under Uncertainty: A Comprehensive Framework

5a. CONTRACT NUMBER
N00014-12-1-0023

5b. GRANT NUMBER

5c. PROGRAM ELEMENT NUMBER

6. AUTHOR(S)
Frangopol, Dan M.

5d. PROJECT NUMBER

5e. TASK NUMBER

5f. WORK UNIT NUMBER

7. PERFORMING ORGANIZATION NAME(S) AND ADDRESS(ES)
Lehigh University
526 Brodhead Avenue, 23B
Bethlehem, PA 18015

8. PERFORMING ORGANIZATION REPORT NUMBER

9. SPONSORING/MONITORING AGENCY NAME(S) AND ADDRESS(ES)
Office of Naval Research
230 South Dearborn
Room 380
Chicago, IL 60604-1595

10. SPONSOR/MONITOR'S ACRONYM(S)
ONR

11. SPONSOR/MONITOR'S REPORT NUMBER(S)

12. DISTRIBUTION/AVAILABILITY STATEMENT
Approved for Public Release; distribution is Unlimited

13. SUPPLEMENTARY NOTES

14. ABSTRACT
This report summarizes the research progress in the project "Integrating SHM and Time-Variant System Performance of Naval Ship Structures for Near Real-Time Decision Making under Uncertainty: A Comprehensive Framework". The work began on December 1st, 2011 with an intensive review of existing literature and practice regarding structural health monitoring (SHM), time-variant performance and reliability of naval ship structures, updating techniques, and decision making under uncertainty.

See report for additional abstract details.

15. SUBJECT TERMS

16. SECURITY CLASSIFICATION OF:			17. LIMITATION OF ABSTRACT	18. NUMBER OF PAGES	19a. NAME OF RESPONSIBLE PERSON
a. REPORT	b. ABSTRACT	c. THIS PAGE			Nicole M. Corali
U	U	U	SAR	71	19b. TELEPHONE NUMBER *(Include area code)* 610-758-4585

INSTRUCTIONS FOR COMPLETING SF 298

1. REPORT DATE. Full publication date, including day, month, if available. Must cite at least the year and be Year 2000 compliant, e.g. 30-06-1998; xx-06-1998; xx-xx-1998.

2. REPORT TYPE. State the type of report, such as final, technical, interim, memorandum, master's thesis, progress, quarterly, research, special, group study, etc.

3. DATES COVERED. Indicate the time during which the work was performed and the report was written, e.g., Jun 1997 - Jun 1998; 1-10 Jun 1996; May - Nov 1998; Nov 1998.

4. TITLE. Enter title and subtitle with volume number and part number, if applicable. On classified documents, enter the title classification in parentheses.

5a. CONTRACT NUMBER. Enter all contract numbers as they appear in the report, e.g. F33615-86-C-5169.

5b. GRANT NUMBER. Enter all grant numbers as they appear in the report, e.g. AFOSR-82-1234.

5c. PROGRAM ELEMENT NUMBER. Enter all program element numbers as they appear in the report, e.g. 61101A.

5d. PROJECT NUMBER. Enter all project numbers as they appear in the report, e.g. 1F665702D1257; ILIR.

5e. TASK NUMBER. Enter all task numbers as they appear in the report, e.g. 05; RF0330201; T4112.

5f. WORK UNIT NUMBER. Enter all work unit numbers as they appear in the report, e.g. 001; AFAPL30480105.

6. AUTHOR(S). Enter name(s) of person(s) responsible for writing the report, performing the research, or credited with the content of the report. The form of entry is the last name, first name, middle initial, and additional qualifiers separated by commas, e.g. Smith, Richard, J, Jr.

7. PERFORMING ORGANIZATION NAME(S) AND ADDRESS(ES). Self-explanatory.

8. PERFORMING ORGANIZATION REPORT NUMBER. Enter all unique alphanumeric report numbers assigned by the performing organization, e.g. BRL-1234; AFWL-TR-85-4017-Vol-21-PT-2.

9. SPONSORING/MONITORING AGENCY NAME(S) AND ADDRESS(ES). Enter the name and address of the organization(s) financially responsible for and monitoring the work.

10. SPONSOR/MONITOR'S ACRONYM(S). Enter, if available, e.g. BRL, ARDEC, NADC.

11. SPONSOR/MONITOR'S REPORT NUMBER(S). Enter report number as assigned by the sponsoring/ monitoring agency, if available, e.g. BRL-TR-829; -215.

12. DISTRIBUTION/AVAILABILITY STATEMENT. Use agency-mandated availability statements to indicate the public availability or distribution limitations of the report. If additional limitations/ restrictions or special markings are indicated, follow agency authorization procedures, e.g. RD/FRD, PROPIN, ITAR, etc. Include copyright information.

13. SUPPLEMENTARY NOTES. Enter information not included elsewhere such as: prepared in cooperation with; translation of; report supersedes; old edition number, etc.

14. ABSTRACT. A brief (approximately 200 words) factual summary of the most significant information.

15. SUBJECT TERMS. Key words or phrases identifying major concepts in the report.

16. SECURITY CLASSIFICATION. Enter security classification in accordance with security classification regulations, e.g. U, C, S, etc. If this form contains classified information, stamp classification level on the top and bottom of this page.

17. LIMITATION OF ABSTRACT. This block must be completed to assign a distribution limitation to the abstract. Enter UU (Unclassified Unlimited) or SAR (Same as Report). An entry in this block is necessary if the abstract is to be limited.

Final Technical Report

December 1st, 2011 to September 30th, 2016

Agreement No. N00014-12-1-0023

Project Title: Integrating SHM and Time-Variant System Performance of Naval Ship Structures for Near Real-Time Decision Making under Uncertainty: A Comprehensive Framework

Submitted to
Dr. Paul E. Hess III
Program Officer, Code 331, ONR Ship Systems and Engineering Division,
Office of Naval Research, 875 N. Randolph St., Arlington, VA 22203
Phone: 703-696-9776 Fax: 703-696-0001 E-mail: hessp@onr.navy.mil

Submitted by
Dr. Dan M. Frangopol
Professor and Fazlur R. Khan Endowed Chair of Structural Engineering and Architecture,
Department of Civil and Environmental Engineering,
Center for Advanced Technology for Large Structural Systems (ATLSS Center),
Lehigh University, 117 ATLSS Drive, Imbt Labs, Bethlehem, PA 18015-4729
Phone: 610-758-6103 Fax: 610-758-4115 Email: dan.frangopol@lehigh.edu

September 30th, 2016

ABSTRACT

This report summarizes the research progress in the project "*Integrating SHM and Time-Variant System Performance of Naval Ship Structures for Near Real-Time Decision Making under Uncertainty: A Comprehensive Framework*". The work began on December 1st, 2011 with an intensive review of existing literature and practice regarding structural health monitoring (SHM), time-variant performance and reliability of naval ship structures, updating techniques, and decision making under uncertainty.

The acquired concepts were used next to investigate the ship structure reliability and redundancy under different operational conditions (i.e., sea states, speeds, and heading angles). Additionally, the work has been extended to investigate methodologies for improving the accuracy of the performance assessment process by implementing the Bayesian updating method. In this approach, SHM signals of the ship are used to find the updated Rayleigh-distributed load effects which are subsequently used to estimate the posterior ship reliability and redundancy with respect to the vertical bending moment. The performance of ship hull under the combined effects of progressive and sudden damage (e.g., due to grounding and collision) is also investigated probabilistically. Additionally, an approach which enables the integration of SHM data to compute the fatigue reliability and service life for structural details of high-speed aluminum vessels is presented. Moreover, a risk-informed approach for the optimal mission oriented routing of ships is developed. The strength of the hull is investigated by modeling the midship section with finite elements and by analyzing different damage levels depending on the propagation of plastification throughout the section. Uncertainties associated with geometry and material properties are accounted for by means of the implementation of the response surface method. Reliability analysis is performed for several ship operational conditions and considering four different limit states. Then, risk is assessed by including the direct losses associated with five investigated damage states. Finally, the optimal routing of ships is obtained by minimizing both the estimated time of arrival and the expected direct risk, which are clearly conflicting objectives. The approach also enables integrating SHM and time-variant system performance for near real-time decision making under uncertainty. The work presented in this report was accomplished by the PI (Dan M. Frangopol) and several current and former doctoral students including Mohamed Soliman (graduated in January 2015), Benjin Zhu (graduated in January 2015), Duygu Saydam (graduated in September 2013), Alberto Decò (graduated in September 2013), You Dong (graduated in May 2016), Samantha Sabatino, and Alysson Mondoro.

TECHNICAL OBJECTIVES

In recent years, engineering practice has been largely impacted by advances in structural health monitoring (SHM). However, there is still an outstanding question of how to optimally plan SHM activities over the service life of deteriorating structures. There has been little research on integration of SHM concepts and technologies into maintenance management and decision-making framework in order to improve system performance of naval ship structures in a more cost-effective manner and to achieve substantial life-cycle cost savings under uncertainty.

The main objective of the project is to develop a comprehensive framework for integrating SHM and time-variant system performance of naval ship structures for near real-time decision making under uncertainty. This project will advance both the state-of-the-art and state-of-practice in equipping naval vessels with real-time monitoring systems that include structural diagnosis and prognosis capabilities to support operational and maintenance decisions for rapid response to various events and optimal maintenance planning.

TECHNICAL APPROACH

The technical approach is based on using the system performance theory coupled with SHM in a unified time-space correlated way. This approach is considered a paramount innovation. Only such a complete reliability-based time-space framework can be a truly useful tool for decision makers. This approach consists of several major tasks, as follows:

1. First, a literature survey of current practice and research findings in SHM, performance and reliability of naval ship structures will be conducted.
2. Methodologies for predicting time-dependent reliability at ship component-level (considering an individual part of a ship only, such as the hull) under different operational conditions (e.g., speed, sea state and heading angle) will be investigated and a computational framework will be developed. The effect of SHM on reliability will be investigated using advanced updating techniques.
3. The component-level framework will be extended to ship system-level considering SHM and system effects both in space and time under uncertainty. The various classes of failures will be grouped based on the consequence using a consistent risk-based approach.
4. Develop a probabilistic framework to optimally plan SHM activities over the service life of deteriorating ships.
5. Integrate SHM and time-variant system performance of naval ship structures for near real-time optimal decision making under uncertainty to support operational and maintenance decisions for rapid response to various events affecting their service life reliability.

PROGRESS STATEMENT SUMMARY

The research started on December 1st, 2011. During the time interval 12-1-2011 to 9-30-2016, the PI and his research team worked on (a) literature survey of current practice and research findings in SHM, performance, and reliability of naval ship structures, (b) the development of methodologies for predicting ship reliability under sudden or progressive damaging effects, and (c) investigating the possible integration of SHM data and the use of advanced updating techniques to improve the accuracy of the performance assessment of ships, (d) investigating approaches for optimally planning SHM activities over the service life of deteriorating ships, and (e) developing a framework to integrate SHM and time-variant system performance of naval ship structures for near real-time optimal decision making under uncertainty. All the objectives of the project were achieved in September 2016.

Methodologies for predicting time-dependent performance of ships considering sudden and progressive damage under different operational conditions are investigated. A computational framework for quantifying the structural reliability and redundancy is developed. Additionally, the effect of integrating SHM information on reliability and redundancy evaluation using advanced updating techniques is investigated. An approach for integrating SHM data to evaluate the reliability of aluminum ship details with respect to fatigue is proposed. Methodologies for the optimal planning of SHM and inspection activities and enhanced near real-time risk-based decision making are also investigated. Application of SHM and updating techniques to support near-real time decision making with respect to ship routing are presented.

PROGRESS

This section presents the major technical research and investigation findings up to September 30th, 2016. It consists of six subsections as follows:

1. Reliability and Redundancy of Ship Structures under Different Operational Conditions
2. Incorporation of Structural Health monitoring Data on Load Effects in the Reliability and Redundancy Assessment of Ship Cross-sections Using Bayesian Updating
3. Performance Assessment of Ship Hulls under Progressive and Sudden Damage
4. Incorporation of Structural Health Monitoring Data to Compute the Fatigue Reliability and Service Life of Aluminum Vessels
5. Risk-informed Optimal Routing of Ships Considering Different Damage Scenarios and Operational Conditions
6. Real-time Risk Assessment of Ship Structures Integrating Structural Health Monitoring Data: Application to Multi-objective Optimal Ship Routing

1. Reliability and Redundancy of Ship Structures under Different Operational Conditions

The proper knowledge of ship structural vulnerability under specific operational conditions is the key to maintain an adequate safety level. Due to time and distance constraints, sometimes vessels are forced to plan routes that put their structure at risk, possibly experiencing dramatic drops of their operational safety. In fact, ship structures are subjected to the effects of the environment in which they operate. Depending on the encountered sea conditions, the load effects on the hull may vary over a journey potentially inducing extreme danger. The assessment of performance indicators that characterize structural safety (such as reliability and redundancy) is crucial (Frangopol *et al.* 2011, Frangopol *et al.* 2012), especially if adverse sea conditions are expected to be encountered. Preventing ship structures under operation from down-crossing predefined safety thresholds leads to avoid potential failures that cause economic losses and loss of lives.

Several studies focused on the assessment of ship reliability associated with ultimate flexural capacity (Mansour and Hovem 1994, Mansour 1997, Ayyub *et al.* 2000, Luís *et al.* 2009). Furthermore, the variation over time of reliability, also associated with ultimate flexural capacity, has been extensively investigated (Paik *et al.* 1998, Guedes Soares and Garbatov 1999, Paik and Frieze 2001, Akpan *et al.* 2002). Ship reliability has been investigated also with respect to flexural capacity associated with the failure of the first element (stiffened plate) within a ship

cross-section (Lua and Hess 2003, Lua and Hess 2006, Decò *et al.* 2011). Although the maximum vertical bending moments (sagging and hogging) generally occur amidship, in order to properly assess the overall ship safety, a system composed by multiple cross-sections is investigated herein.

Even if few comprehensive studies have been conducted for the evaluation of structural performance and mostly focusing on performance-based design other than safety estimates (Glen *et al.* 1999, Dinovitzer 2003), literature lacks in studies that assess structural reliability and redundancy of ships under different operational conditions, including aging consideration. This investigation provides a comprehensive study reporting on ship reliability and redundancy for a wide spectrum of operational options.

In this study, the polar plots are used to represent reliability and redundancy indices associated with heading angles from 0 (head sea) to 180 degrees (following sea) for both sagging and hogging. As indicated in Decò et al. 2012, since the ship structure is quasi-symmetric, heading angles θ and $-\theta$ are likely to provide very similar values of the reliability index; therefore, only one half of the graph is plotted for hogging and the other half for sagging. The assumption is made only to condensate more information in a single graph. The reliability index in Figure 1 is shown qualitatively for a specific cross-section of the ship, a specific sea state, and a specific limit state (i.e., a single failure mode or a combination of failure modes). Combining data on multiple cross-sections, it is also possible to plot the lowest reliability index among all the cross-sections in a single polar plot.

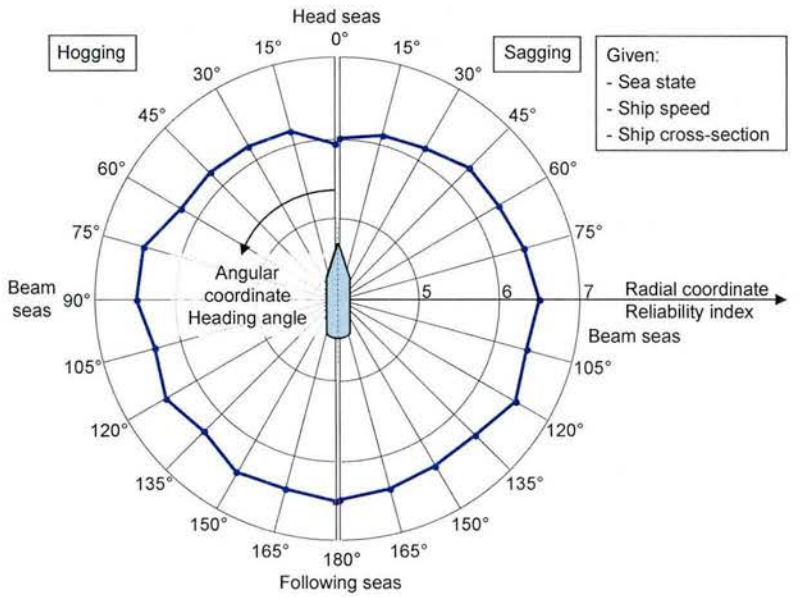

Figure 1 Qualitative polar plot of the reliability index for a specific cross-section of the ship versus the heading angle. The left part of the plot is associated with hogging and the right part with sagging. The sea state, speed, and cross-section of the ship are all specified.

The next sections describe the loading and resistance models used in this investigation along with research outcomes and conclusions.

1.1. Loading Model

The effects induced by the sea on the hull are due to still water and induced by waves. Safety evaluation of ship structures operating in different sea and cargo conditions requires a probabilistic estimation of the load effects due to still water and waves (Guedes Soares 1992). Since design considerations are not the goal of this study, "long-term" statistics are not accounted for. This study provides indications on the assessment of structural safety of ships undergoing different operational conditions without making any assumption on the possible ship routes, therefore "short-term" (i.e., mission oriented) loads are quantities of interest.

1.1.1. Still water bending moment

The adopted probabilistic model for the evaluation of the vertical bending moments (VBM) due to still water relies on the method proposed by Hussein and Guedes Soares (2009). Since detailed information regarding the location and magnitude of the loads within the vessel is generally not available or seldom recorded, the methodology is based on conservative rule values, such as those provided in IACS (2008). Accordingly, the VBMs $M_{sw,sag,CS}$ and $M_{sw,hog,CS}$ (sagging and hogging, respectively) for a specific ship cross-section (CS) are (IACS 2008):

$$M_{sw,sag,CS} = f_{sw,CS}\, 0.05185 C_{wv} l^2 b (C_b + 0.7) \qquad \text{for sagging} \qquad (1)$$

$$M_{sw,hog,CS} = f_{sw,CS}\, 0.01 C_{wv} l^2 b (11.97 + 1.9 C_b) \qquad \text{for hogging} \qquad (2)$$

where $f_{sw,CS}$ is the factor accounting for the variation of VBMs along the vessel length (with 1.0 at midship), C_b is the ship block coefficient, l is the ship length (m), b is the ship breadth (m), and C_{wv} is a wave coefficient calculated as follows (IACS 2008):

$$C_{wv} = \begin{cases} 10.75 - \left(\dfrac{300 - l}{100}\right)^{\frac{3}{2}} & \text{for } 150 \le l \le 300 \\ 10.75 & \text{for } 300 < l \le 350 \\ 10.75 - \left(\dfrac{l - 350}{150}\right)^{\frac{3}{2}} & \text{for } 350 < l \le 500 \end{cases} \qquad (3)$$

The maximum still water bending moments can be taken as 90% of those obtained by common rules (e.g. IACS 2008). Hussein and Guedes Soares (2009) proposed the use of a normal

distribution with mean and standard deviation to be taken as 70% and 20% of the maximum still water bending moment, respectively.

1.1.2. Wave-induced bending moment

This investigation focuses on the evaluation of VBM of ships subjected to different operational conditions by applying the linear method. Estimates of VBM must be provided for each investigated ship operational condition, represented by a group of input parameters such as sea states, ship speeds and headings.

The structural responses for regular waves become crucial when assessing the ship response due to natural sea given by linear superposition. Responses for single waves are based on hydrodynamic analyses of the ship in case of having steady conditions (steady harmonic variation of the loads on the structure), disregarding the transient effects (Faltinsen 1990). Forces and moments on ships induced by waves mostly rely on hydrodynamic rather than structural analysis. Generally, hydrodynamic analyses are complex tasks that involve the use of computer-based tools, and abundantly lay outside the common role of ship structural engineers (Hughes 1983). A relatively simple technique to perform hydrodynamic analysis of operating vessels is based on strip theory or strip method (Korvin-Kroukowski and Jacobs 1957). With respect to other techniques, simplifications are introduced by the strip theory, in which the ship hull is divided into prismatic segments (strips). Hydrodynamic forces induced by harmonic waves are evaluated within the individual segments, disregarding any interaction between adjacent ones. Then, shear and bending moment within the entire hull are evaluated by integrating the obtained hydrodynamic forces along the segments (Hughes 1983). This method relies on a two-dimensional flow theory, therefore interaction between segments is neglected.

Although commercial software packages performing linear analysis are available, freeware software developed by field specialists or academic institutions is also accessible. For instance, the freeware program PDSTRIP (2006) developed in FORTRAN language has been proven to be a useful tool computing the seakeeping of ships and other floating bodies according to the strip method (Bertram *et al.* 2006, Palladino *et al.* 2006).

One of the key points while using linear theory for the determination of hull loads is obtaining the Response Amplitude Operator (RAO) from ship hydrodynamic analysis. In this study, VBM RAOs are of interest. While dealing with time-varying processes, their representation in terms of spectral density function can be a great advantage, especially for the response analysis of linear systems. In this case, if both the input $X(t)$ and output $Y(t)$ of the system are expressed by spectral density functions, their relation is associated with the transfer function $\Phi(\omega)$ as follows (Hughes 1983):

$$S_Y(\omega) = |\Phi(\omega)|^2 S_X(\omega) \tag{4}$$

where $S_Y(\omega)$ and $S_X(\omega)$ are the spectral density functions of the output and input, respectively; and ω is the circular frequency (rad/s).

The ocean surface is extremely irregular and the prediction of wave configurations is a complex issue. In this context, statistical tools can provide the basis for a probabilistic study of the structural response for ships in natural sea (irregular sea). The mathematical representation of the sea surface becomes feasible and relatively simple when the problem is solved linearly. Practically, this allows to evaluate the ship structural response for each individual regular wave, and thus to obtain statistical estimates by superposing the results of a large number of waves. Since the instantaneous value of the ocean elevation follows a Gaussian distribution, and in accordance with Faltinsen (1990), the probability density function (PDF) of the peak values of the wave elevation A_w is assumed to be described by the Rayleigh distribution, defined as:

$$f(A_w) = \frac{A_w}{m_0} \exp\left(-\frac{A_w^{\,2}}{2m_0}\right) \tag{5}$$

where m_0 is the zero-*th* moment of the wave spectrum S_W (i.e., the area under the spectrum), expressed as (Hughes 1983):

$$m_0 = \int_0^\infty \omega^0 S_W(\omega)\mathrm{d}\omega \tag{6}$$

Various sea spectra are adopted in numerous studies, depending on ocean/sea characteristics (Michel 1999). In this investigation, the spectrum for fully developed sea, suggested by the International Ship and Offshore Structures Congress (ISSC) and representing a modified version of the Pierson-Moskowitz sea spectrum, is selected (Faltinsen 1990):

$$S_{W,SS}(\omega) = \frac{0.11}{2\pi}\left(\frac{\omega T_1}{2\pi}\right)^{-5} \exp\left[-0.44\left(\frac{\omega T_1}{2\pi}\right)^{-4}\right] H_{1/3}^2 T_1 \tag{7}$$

where $S_{W,SS}(\omega)$ is the sea spectrum for a given sea state *SS*, T_1 is the wave mean period (s), and $H_{1/3}$ is the significant wave height corresponding to the mean of the one third highest waves (m). The sea state scale for wind sea plays a fundamental role for the evaluation of the load magnitude. The values of the wave mean period and significant height depend upon the intensity of the sea states.

For long crested sea and for low frequency waves, the correlation coefficients between two loads components denoted *i* and *j* are given by (Mansour and Thayamballi 1994):

$$\rho_{ij} = \frac{1}{\sigma_i \sigma_j} \int_0^\infty \mathrm{R}\left[\Phi_i(\omega)\Phi_j^*(\omega)\right] S_W(\omega) d\omega \tag{8}$$

where $\Phi_i(\omega)$ is the transfer function of load component i, $\Phi_j^*(\omega)$ is the complex conjugate of the transfer function of load component j, $S_W(\omega)$ is the sea spectrum, σ_i and σ_j are the individual standard deviations, and R denotes the real part of the complex quantity within parenthesis.

Once RAO curves for wave-induced VBM $M_{w,CS,SS,U,H}$ are obtained for each considered operational condition and each section, the response spectrum $S_{M,CS,SS,U,H}(\omega_e)$ can be obtained as (Hughes 1983):

$$S_{M,CS,SS,U,H}(\omega_{e,U,H}) = \left|\Phi(\omega_{e,U,H})\right|^2 S_{W,SS}(\omega_{e,U,H}) \tag{9}$$

For a linear system, once the response spectra for the VBMs are evaluated, the associated PDF of the Rayleigh distributions of the investigated structural response considering several operational conditions is provided (Hughes 1983):

$$f(M_{w,CS,SS,U,H}) = \frac{M_{w,CS,SS,U,H}}{m_{0,CS,SS,U,H}} \exp\left(-\frac{(M_{w,CS,SS,U,H})^2}{2m_{0,CS,SS,U,H}}\right) \tag{10}$$

Thus, the relevant descriptor of the probability distribution of the VBM (mode α) is:

$$\alpha(M_{w,CS,SS,U,H}) = \sqrt{m_{0,CS,SS,U,H}} \tag{11}$$

The mean μ_r and standard deviation σ_r are (Papoulis 1984):

$$\mu_r(M_{w,CS,SS,U,H}) = \sqrt{\frac{\pi}{2}}\alpha(M_{w,CS,SS,U,H}) \tag{12}$$

$$\sigma_r(M_{w,CS,SS,U,H}) = \sqrt{\frac{4-\pi}{2}}\alpha(M_{w,CS,SS,U,H}) \tag{13}$$

1.2. Reliability and Redundancy Indices

The quantitative evaluation of the safety of the hull is based on reliability and redundancy indicators. The level of safety depends on both the strength of the hull and ship operational conditions. Although ship reliability is generally assessed only amidship, in this study, several cross-sections are investigated in order to enhance the assessment of hull safety by using a system-oriented procedure.

Ship reliability analysis can be performed based upon the knowledge of the probability distributions of loads and resistances for each cross-section (following the methods previously explained) and including model (i.e., epistemic) uncertainties. The failure probabilities and the corresponding reliability indices, with respect to flexural capacities associated with a specific cross-section *CS*, are based on the following limit state equations (Paik and Frieze 2001):

$$G_{UF,sag,CS,SS,U,H}(t) = x_R UFM_{sag,CS}(t) - x_{sw} M_{sw,sag,CS} - x_w M_{w,CS,SS,U,H} = 0 \quad (14)$$

$$G_{UF,hog,CS,SS,U,H}(t) = x_R UFM_{hog,CS}(t) - x_{sw} M_{sw,hog,CS} - x_w M_{w,CS,SS,U,H} = 0 \quad (15)$$

$$G_{FF,sag,CS,SS,U,H}(t) = x_R FFM_{sag,CS}(t) - x_{sw} M_{sw,sag,CS} - x_w M_{w,CS,SS,U,H} = 0 \quad (16)$$

$$G_{FF,hog,CS,SS,U,H}(t) = x_R FFM_{hog,CS}(t) - x_{sw} M_{sw,hog,CS} - x_w M_{w,CS,SS,U,H} = 0 \quad (17)$$

where the subscripts *UF*, *FF*, *sag*, *hog*, *CS*, *SS*, *U*, and *H* refer to ultimate failure, first failure, sagging, hogging, ship cross-section, sea state condition, ship speed, and ship heading, respectively; $G_{UF,sag,CS,SS,U,H}(t)$, $G_{UF,hog,CS,SS,U,H}(t)$, $G_{FF,sag,CS,SS,U,H}(t)$, and $G_{FF,hog,CS,SS,U,H}(t)$ are the time-dependent performance functions; $UFM_{sag,CS}(t)$ and $UFM_{hog,CS}(t)$ are time-dependent ultimate failure bending moments, $FFM_{sag,CS}(t)$ and $FFM_{hog,CS}(t)$ are time-dependent first failure bending moments; $M_{sw,sag,CS}$ and $M_{sw,hog,CS}$ are the still water bending moments, $M_{w,CS,SS,U,H}$ is the wave-induced bending moment given by linear theory; x_R, x_{sw}, and x_w are the model uncertainties associated with the resistance determination, still water bending moment prediction, and wave-induced bending moment prediction, respectively. The ultimate capacity of the ship hull sections is evaluated using the approach proposed by Okasha and Frangopol (2010).

The assessment of the time-variant redundancy index is necessary in order to study the behavior of structures prone to sudden failure. A redundant system is a system able to redistribute the loads throughout multiple components even though one or more components fail (Frangopol 2011). Decò *et al.* (2011) investigated redundancy of ship structures based on the following reliability-based time-variant redundancy definitions:

$$RI_1(t) = \frac{P_{f,FF}(t) - P_{f,UF}(t)}{P_{f,UF}(t)} \quad (18)$$

$$RI_2(t) = \beta_{UF}(t) - \beta_{FF}(t) \quad (19)$$

where $P_{f,UF}(t)$ and $P_{f,FF}(t)$ are the failure probabilities associated with the ultimate failure of a cross-section and the failure of the first stiffened plate within a cross-section, respectively; and

$\beta_{UF}(t)$ and $\beta_{FF}(t)$ are the corresponding reliability indices. The relationship between the reliability index β and the failure probability P_f is:

$$\beta = \Phi^{-1}\left(1 - P_f\right) \tag{20}$$

where Φ^{-1} is the inverse standard normal distribution function.

1.3. Illustrative Example

Reliability and redundancy indicators under different operational conditions are assessed for the Joint High-Speed Sealift (JHSS) discussed in Devine (2009). Figure 2(a) shows the 3-D geometrical model obtained by using the software FREE!ship (2006). Three representative transversal ship cross-sections, denoted *CS*1 (fore quarter point 72.5 m aft FP), *CS*2 (midship 145 m aft FP), and *CS*3 (aft quarter point 217.5 m aft FP) have been investigated. The load effects induced by still water in terms of VBM are evaluated based on the conservative rule values provided in IACS (2008) and given by applying Eqs. (1) and (2) for sagging and hogging, respectively.

RAO curves and load descriptors (based on Rayleigh distribution) are evaluated with respect to the VBM for each of the three ship cross-sections (in Figure 2) and for each operational condition. Since the JHSS is a fast naval vessel, and assuming that the maximum forward speed can reach up to 20 m/s (38.9 knots), the following five speeds are considered: 0 m/s (0 knots), 5 m/s (9.7 knots), 10 m/s (19.4 knots), 15 m/s (29.2 knots), and 20 m/s (38.9 knots). Ship structural performances are evaluated for different ship headings. Angles between 0° (following sea) and 180° (head sea) by multiples of 20° are accounted for.

Cross-section geometries are managed by a developed MATLAB (The MathWorks 2009) code that converts the exported file to a suitable format for the software PDSTRIP (2006) in order to perform linear response analysis under regular waves (strip theory). VBMs for the three ship cross-sections are obtained with respect to different waves having unitary amplitude and length between 24 m and 1300 m (95 values irregularly spaced). A large number of wave lengths is necessary in order to achieve enough values to build the RAO curves with sufficient accuracy. Moreover, the input file of PDSTRIP allows accounting for different ship speeds and headings.

Once RAOs have been obtained, by selecting a sea spectrum (given by Eq. (8) after inputting specific significant wave height and average wave period) and by applying Eq. (9), the response spectra can be assessed. According to Rayleigh distribution, for each considered operational condition it is possible to evaluate the mode, mean, and standard deviation of the response distribution given by Eqs. (11), (12), and (13), respectively.

According to Eq. (6), the values of the loads are proportional to the areas subtended by the response spectrum curves. Figure 3(a) shows the polar representation of the vertical bending moment (VBM) for the three ship cross-sections (*CS*1, *CS*2, and *CS*3) in the case of sea state 6

and speed of 5 m/s. Obviously, the highest load effects are found for the cross-section amidship (*CS*2) and lower load values for the other two cross-sections at quarter points. Figure 3(b) gives indications about the dispersion of the VBM for the cross-section amidship by showing the profiles of the mean μ and mean plus and minus one standard deviation σ, ($\mu+\sigma$ and $\mu-\sigma$, respectively) in case of sea state 6 and no speed (U = 0 m/s). VBM responses associated with beam sea (90° and 270°) become insignificant. Figure 3(c) shows the effects on the mean VBM for *CS*2 due to the variation of speed under sea state 5.

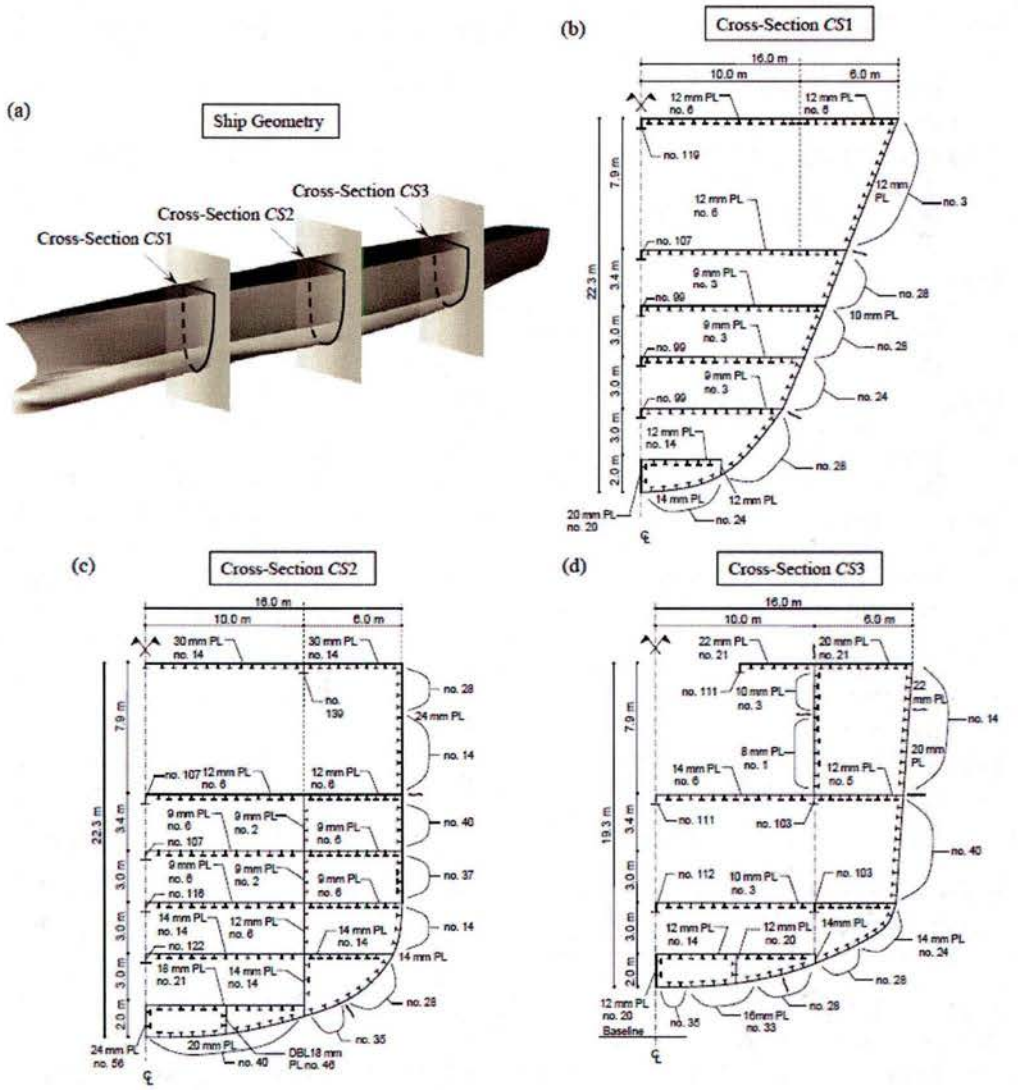

Figure 2 (a) Geometrical model of the analyzed JHSS developed by the software FREE!ship (2006). Geometry of (b) cross-section 1 (*CS*1), (c) cross-section 2 (*CS*2), and (d) cross-section 3 (*CS*3).

Although the use of a linear approach provides conservative approximated results (Ayyub *et al.* 1998), improved results can be obtained by applying methods that accounts for non-linearity in the wave-induced loading as well as vibration effects such as springing and whipping loads, usually associated with high frequency excitations. These effects are here neglected, being their evaluation outside the scope of this case study. Due to linear theory, the resulting bending moments are the same for both sagging and hogging (Hughes 1983, Lua and Hess 2006) and the results shown in the polar plots can be affected by inaccuracy, especially when the responses are concentrated in very low or very high encountered frequencies. Profiles are also affected by the error made while discretizing the input data, sometimes leading to sharp angles.

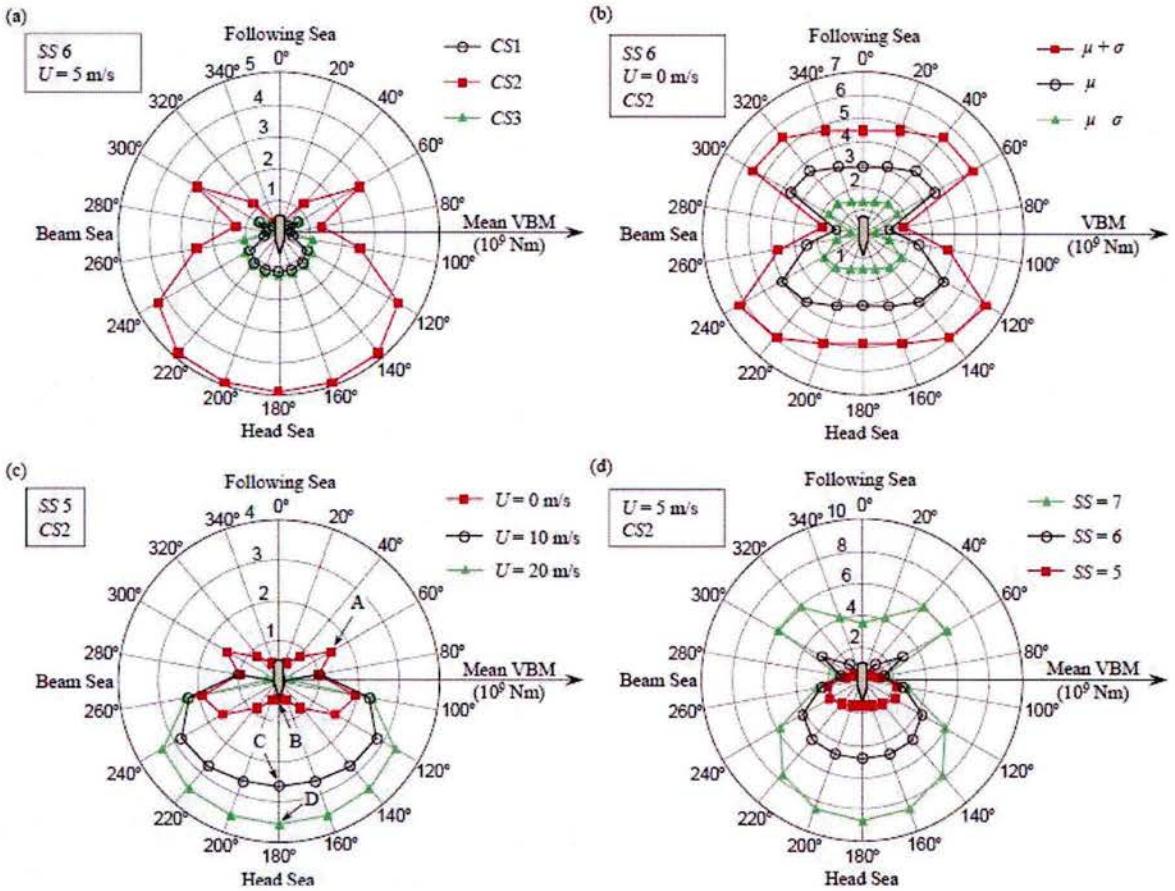

Figure 3 Polar representation of the VBM. (a) Profiles of mean VBM for different cross-sections, (b) profiles of mean and mean plus and minus one standard deviation of the VBM, (c) profiles of mean VBM for *CS*2 and sea state 5 by varying ship speed, and (d) profiles of mean VBM for *CS*2 and ship speed of 5 m/s by varying sea state. Plots of mean VBM (e) for different cross-sections and (f) for *CS*2 by varying sea state.

The time-variant redundancy indices are calculated according to Eq. (18), and based upon the assessment of the failure probabilities associated with first and ultimate flexural failures. By investigating the same operational conditions as those previously investigated, a similar polar representation for redundancy (sagging and hogging) is shown in Figure 4. These plots consider the same operational conditions as those used in Figure 3.

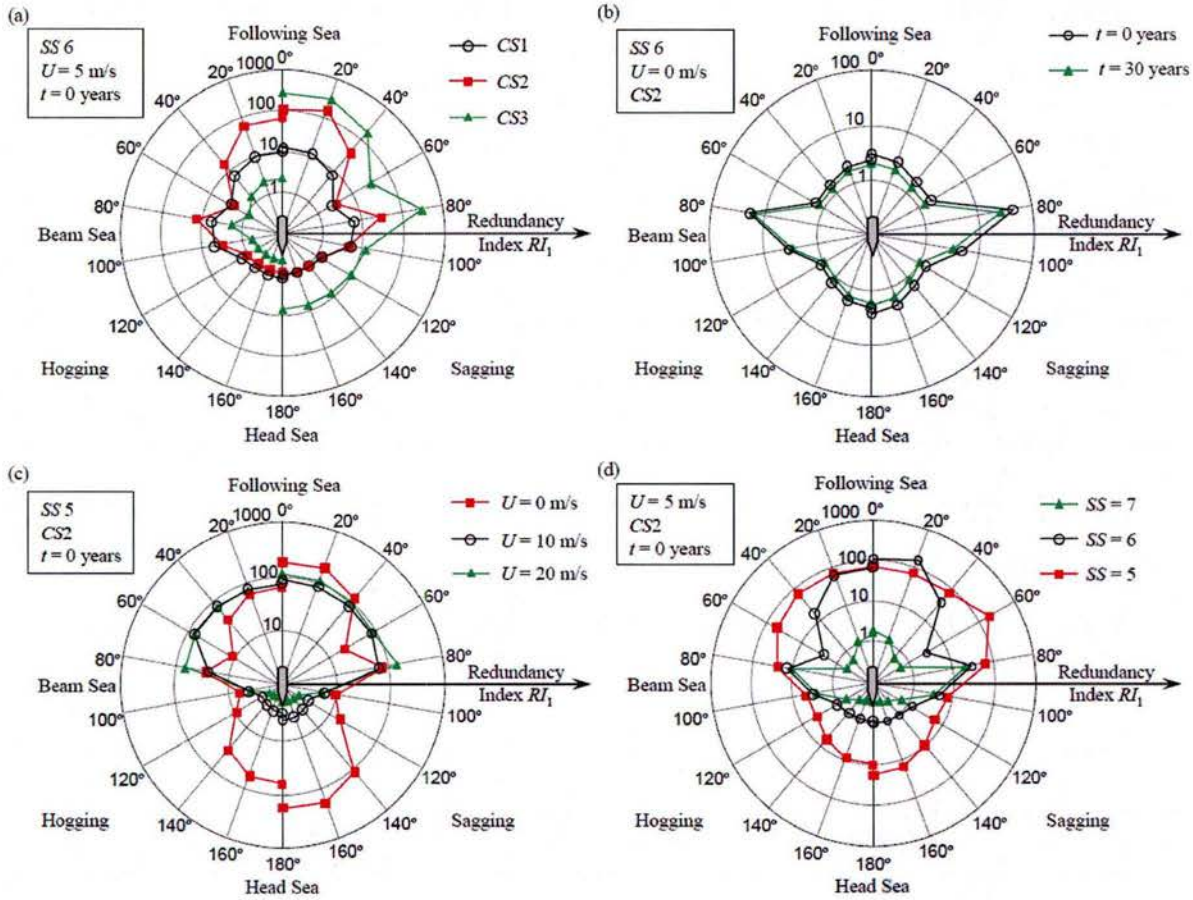

Figure 4 Polar representation of the redundancy index RI_1 given by Eq. (18) associated with ultimate failure for sagging and hogging. (a) Profiles of the redundancy index for different cross-sections, (b) profiles of the redundancy index for the intact structure (year 0) and aged structure (year 30), (c) profiles of the redundancy index for *CS*2 and sea state 5 by varying ship speed, (d) and profiles of the redundancy index for *CS*2 and ship speed of 5 m/s by varying sea state.

It can be noticed from Figure 4(a) that redundancy in sagging for *CS*3 is much higher than the one in hogging, due to the geometry of this cross-section. In fact, the upper part of the cross-section is interrupted and most of the inertia is concentrated at the bottom part of the cross-section leading to worse performance in hogging. Generally, redundancy of *CS*2 is greater than

that of *CS*1 for both sagging and hogging as reported in Figure 4(a). According to Figure 4(b), the redundancy profile of an aged structure (year 30) is a scaled offset of the profile for the intact case (year 0). Furthermore, it is found that redundancy decreases to critical values when the ship speed increases from 0 to 20 m/s, especially for head sea (see Figure 4(c)). Redundancy dramatically decreases also when the sea state becomes more severe (from sea state 5 to 7) as shown in Figure 4(d). According to investigation outcomes, very similar results are obtained by adopting the definition of redundancy provided in Eq. (19).

1.4. Conclusions

Ship lifetime safety can be estimated upon assessing ship structural performance for a large spectrum of operational conditions. Maintaining a specific speed and heading angle for different sea states may lead to dangerous structural performance, putting at risk the integrity of the whole ship and crew lives. This investigation presents an efficient approach for the evaluation of ship reliability and redundancy. This approach allows to investigate aging vessels accounting for the deterioration of their performance over time due to corrosion effects.
The following conclusions are obtained:

1. The proposed polar representation for reliability and redundancy improves the interpretation of the structural safety level under specific operational conditions, helping the ship operator make appropriate decisions.
2. In the case of hogging, it has been found that the cross-sections *CS*1 and *CS*2 have lower redundancy than that of amidship (i.e., cross-section *CS*2). However, reliability indices of the three ship cross-sections are quite similar, indicating that the design is adequate for the hull cross-sections.
3. It can be noted that some operational conditions lead to significant drop of redundancy. When the structural performance reaches a set threshold (warning situation), operational conditions must be modified according to the residual structural safety by reducing the forward speed, or by changing the heading angle in order to improve the structural performance.
4. The proposed framework could be enhanced by including structural health monitoring (SHM) technologies able to provide further information regarding "real time" stresses in the hull. As shown in the next subsection, the proposed study can accommodate SHM by means of updating the prior information with new obtained datasets.

2. Incorporation of Structural Health Monitoring Data on Load Effects in the Reliability and Redundancy Assessment of Ship Cross-sections Using Bayesian Updating

During the performance assessment and prediction of ship structures, the results are usually very sensitive to changes in the input parameters associated with the mechanical models and load conditions (Frangopol et al. 2012). Therefore, objective information on the real conditions of the ship strength and loadings is helpful in reducing the uncertainty in the results. Structural health monitoring (SHM) is a powerful technology that can collect reliable data about the ship

responses to various operational conditions, detect the emergence of damages, and perform real-time diagnosis of the ship structural behavior (Devine 2009, Okasha et al. 2011). The data acquired from SHM are usually limited in most circumstances and how to make efficient use of these data is particularly important. In such a case, Bayesian estimation approach is recommended since it can combine the judgmental information with objective SHM data to obtain a balanced estimation (Ang and Tang 2007).

The objective of this investigation is to present an approach for reducing the uncertainty in the reliability and redundancy assessment of ship cross-sections using the Bayesian updating method. The results presented in this report are those presented in Zhu and Frangopol (2013). Since the information on the ship routes is usually not available, the loading condition in this investigation is considered as "short-term". The prior load effects of the wave-induced bending moments are calculated for different heading angles based on the linear theory. After extracting the hogging and sagging peaks from the low frequency signals, the Bayesian method is used to update the Rayleigh-distributed prior load effects. The original and updated reliability and redundancy indexes associated with the investigated cross-sections for both hogging and sagging are evaluated and the results are displayed in polar plots.

One of the major aspects in the assessment of ship performance is the calculation of the load effects on ship structures due to still water and waves. According to Guedes Soares and Teixeira (Guedes Soares and Teixeira 2000), the primary load effects within the hull girder are the hogging and sagging vertical bending moments. The approach presented in IACS (2008) to approximately estimate the hogging and sagging vertical bending moments for a given transverse cross-section is used in this investigation. In order to consider the uncertainties in the estimation of still water bending moment, Hussein and Guedes Soares (Hussein and Guedes Soares 2009) proposed the use of a normal distribution with the mean and standard deviation to be taken as 70% and 20% of the maximum bending moment which is considered as 90% of the moment obtained by common rules IACS (2008). The resistance estimation model presented in the previous section is also adopted in this study. Additionally, the reliability and redundancy computational approach proposed above and adopted in Okasha and Frangopol (2010), Decò et al. (2011, 2012) is used in this study.

2.1. Bayesian updating

Structural health monitoring has been proved to be a very powerful technique for collecting reliable information about the load effects acting on the ship structures and their responses to various operational conditions (Devine 2009, Okasha et al. 2011). If there is a large amount of observed data, classical approach is used to estimate the statistical descriptors of the distributions. However, when the available data are limited, as is often the case in structural engineering, the Bayesian approach which combines the judgmental information with the objective data will yield better estimation results. Different from the classical approach where the distribution parameters are considered as deterministic, the Bayesian approach solves the estimation problem from another point of view: it deals with the uncertainty by treating the

unknown parameters as random variables. In such a way, all sources of uncertainty related to the estimation of the parameters can be combined using the total probability theorem (Ang and Tang 2007).

Let $f_X(x)$ be the probability density function (PDF) of an underlying random variable X. The parameter of $f_X(x)$, denoted as θ, is considered as a random variable herein and thus is described by a prior PDF $f'(\theta)$. Given a set of observation points (x_1, x_2, …, x_n) acquired from SHM, the likelihood function $L(\theta)$ is constructed by multiplying the PDFs of X evaluated at these SHM data values:

$$L(\theta) = \prod_{i=1}^{n} f_X(x_i \mid \theta) \tag{21}$$

where n is the size of the observed samples. Based on the Bayes theorem, the posterior density function of the parameter θ, $f''(\theta)$, is calculated as follows:

$$f''(\theta) = kL(\theta)f'(\theta) \tag{22}$$

where k is a normalizing constant, given as:

$$k = \left[\int_{-\infty}^{\infty} L(\theta)f'(\theta)d\theta\right]^{-1} \tag{23}$$

Accounting for the uncertainty in the estimation of the parameter θ and the inherent variability of the underlying random variable X, the updated PDF of X, $f'_X(x)$, is obtained using the total probability theorem:

$$f'_X(x) = \int_{-\infty}^{\infty} f_X(x \mid \theta)f''(\theta)d\theta \tag{24}$$

The distribution $f'_X(x)$ can be interpreted as a weighted average of all possible distributions $f_X(x \mid \theta)$ which are associated with different values of θ (Benjamin and Cornell 1970). It is noted from Eq.(22) that: (1) the parameter θ is not included in the final expression of $f'_X(x)$ since it has been "integrated out" of the equation; and (2) as more SHM data become available, the uncertainty associated with the estimation of the distribution of the parameter θ will be reduced and therefore $f'_X(x)$ will be closer to the true distribution of X (Benjamin and Cornell 1970).

Since the closed-form solutions for $f'_X(x)$ are difficult to obtain in most practical cases, a more feasible approach to find an approximate solution for $f'_X(x)$ provided in Okasha *et al.* (2010) is used herein. This approach consists of two steps: (1) calculate the cumulative distribution function (CDF) of the underlying random variable X by performing numerical integration of $f'_X(x)$:

$$F'_X(z_i) = \int_{-\infty}^{z_i}\int_{-\infty}^{\infty} f_X(u \mid \theta)f''(\theta)d\theta du \qquad i = 1,2,...,k \tag{25}$$

where Z =[z_1, z_2, …, z_i, …, z_k] is an array of values whose lower and upper bound is small and large enough, respectively, to cover the range of all probable values of X; moreover, the interval between z_i and z_{i-1} should be small enough to guarantee the precision of the approximate

solution; and (2) perform distribution fitting to the values obtained from Eq. (25) using the method of least square to determine the distribution parameters (Okasha *et al.* 2010).

2.2. Illustrative example

The Joint High Speed Sealift (JHSS), described in the previous section, is presented herein as a case study to demonstrate the process of assessing the reliability and redundancy of ship cross-sections and updating these performance indicators using the collected SHM data. The reliability and redundancy of different cross sections can be evaluated based on the operational condition as mentioned previously.

In this report, Stations 5, 10 and 15 are investigated in the cross-section reliability and redundancy analysis. The SHM data associated with these stations are needed for the updating of the cross-section performance. However in the seakeeping loads test, Stations 5 and 15 were not monitored and the sections where the strains were measured are Stations 4, 7, 10, 13 and 16. Therefore, in order to demonstrate the updating process, the SHM data collected at Stations 4 and 16 are approximately used as the data at Stations 5 and 15 to update their prior load effects based on the fact that Stations 4 and 16 are close to Stations 5 and 15, respectively.

The load effects generated by sea waves consist of wave-induced bending moments associated with low frequency waves and slamming, springing and whipping effects related to high frequency excitations. In order to update the wave-induced bending moments, the low frequency signals are separated from the scaled SHM raw signals using the Butterworth filter in MATLAB signal processing toolbox (Mathworks 2009) and then the positive and negative peaks which correspond to hogging and sagging bending moments are extracted from the filtered low frequency signals.

The available SHM data for the three cross-sections are associated with the operational case of sea state 7, ship speed 35 knots and heading angle 0°. Therefore, only the points associated with this operational case can be updated. During the Bayesian updating of the Rayleigh-distributed VBM, the distribution parameter α is treated as a random variable. Since α is always positive, it is considered to follow a lognormal distribution whose mean value μ_α is determined using the program PDSTRIP (PDSTRIP 2006) and coefficient of variation is assumed to be 10%. For the given operational condition (sea state 7, ship speed 35 knots and heading angle 0°), the mean values μ_α for Stations 5, 10 and 15 are 2.21×10^8, 5.69×10^8 and 4.47×10^8, respectively. By performing the signal filtering and peaks extraction, 406, 397 and 369 hogging and sagging peaks are obtained for Stations 4, 10 and 16, respectively. Based on Eqs. (21-23), the extracted VBM peaks are integrated with the prior PDFs and the samples of the posterior PDFs of α for the three sections are generated using the slice sampling algorithm. After analyzing the results, it was found that these posterior samples are best modeled by the lognormal distributions.

Figure 5 shows the generated samples and fitted PDF associated with Station 15 for both hogging and sagging. The prior and posterior PDFs of the parameter α related to Stations 5, 10 and 15 are plotted in Figure 6. Since the mean values of the prior PDFs are determined based on linear theory, the prior PDFs shown in Figure 6 are the same for both hogging and sagging. However, the hogging and sagging peaks acquired from SHM data may be not the same and this might lead to the difference in the updated posterior PDFs between hogging and sagging.

It is noticed from Figure 6 that (1) the posterior PDFs associated with hogging and sagging are different at Stations 10 and 15 but almost the same at Station 5; (2) for Stations 10 and 15, the mean values of the posterior PDFs for hogging are larger than those for sagging; (3) after integrating with the SHM data, both the mean value and standard deviation of the parameter α at Station 5 are decreased; similar finding is also obtained at Station 15; and (4) for the midship section (Station 10), the mean value of α increases while the standard deviation decreases after updating. The decreases in the dispersion of the parameter in the three stations indicate that integration of the SHM data dramatically reduces the uncertainties in the parameter α for all these cross-sections.

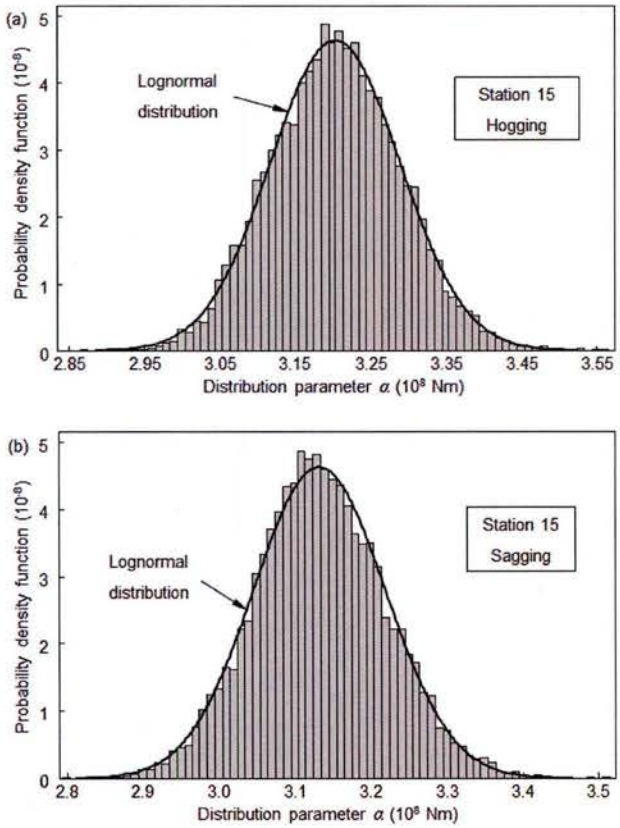

Figure 5 Histogram and fitted PDF of the generated posterior samples of parameter α in Rayleigh distribution associated with Station 15 for (a) hogging; and (b) sagging.

The updated PDFs of the vertical bending moment can be determined by first obtaining the CDF of the VBM based on Eq. (24) and then performing the distribution fitting to estimate the associated parameters. The original and updated PDFs and the SHM data for the three cross-sections are shown in Figure 7. It is found from Figures 7 that (1) the mean and standard deviation associated with Stations 5 and 15 are reduced after the parameter α is updated; while for Station 10 the updated mean VBM is slightly increased; and (2) the difference in the updated PDF between hogging and sagging is very slight for all the sections.

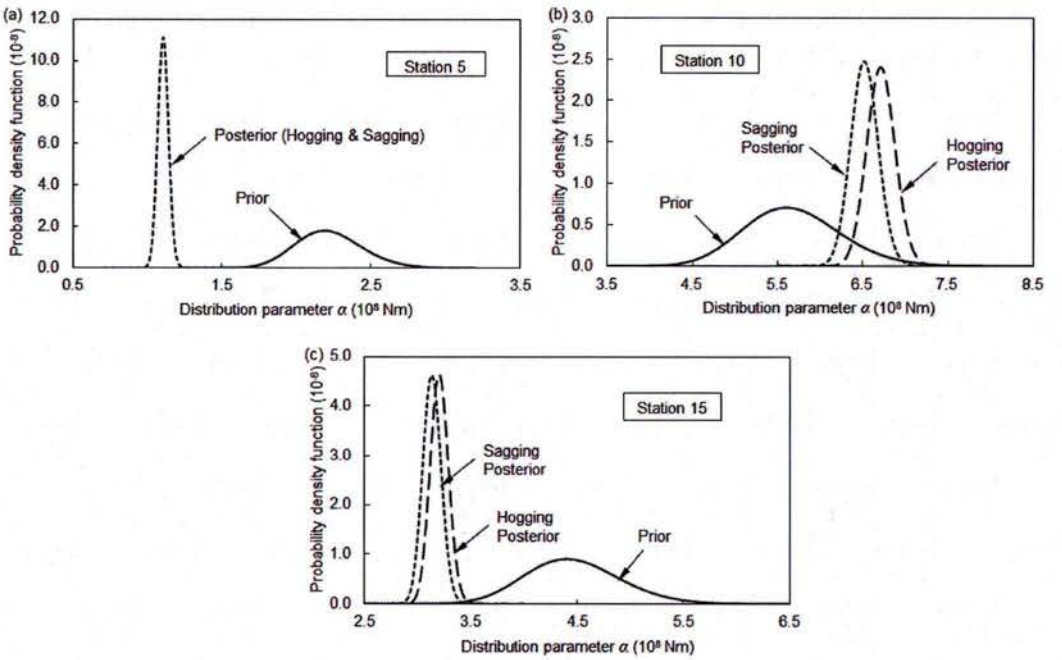

Figure 6 Prior and posterior PDFs of the parameter α in Rayleigh distribution associated with: (a) Station 5; (b) Station 10; and (c) Station 15.

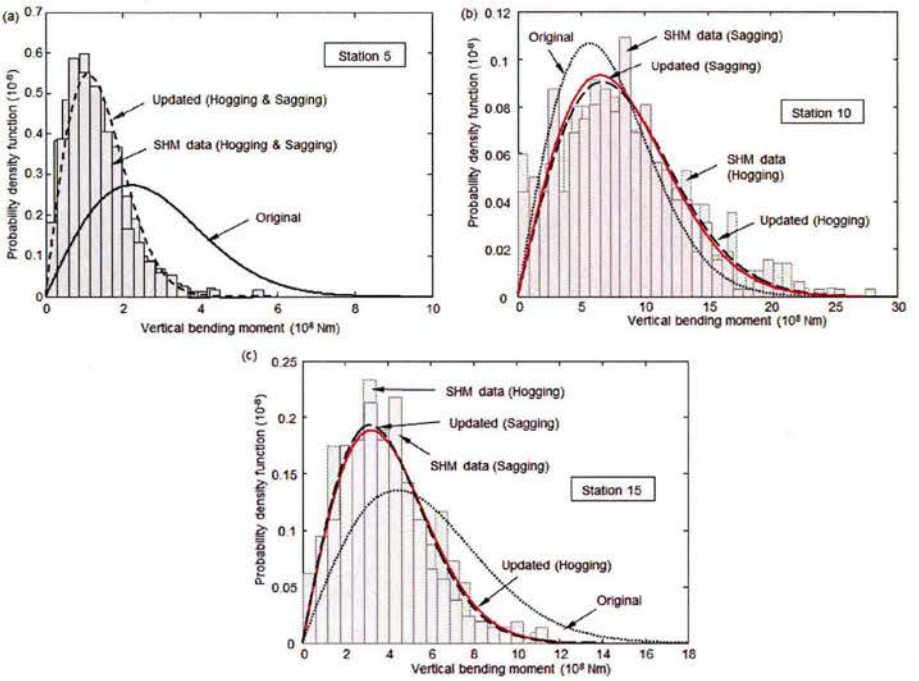

Figure 7 Original and updated PDFs of vertical bending moment associated with: (a) Station 5; (b) Station 10; and (c) Station 15.

Figure 8 shows the updated reliability indexes for heading angle 0° and the original reliability indexes for different heading angles associated with three cross-sections. As shown in the figure, the updated reliability indexes in Stations 5 and 15 are increased for both hogging and sagging cases at the heading angle 0°; while in Station 10, the updated reliability indexes are slightly smaller than the originals. Similarly, the updated redundancy index profiles can be established as indicated in Zhu and Frangopol (2013).

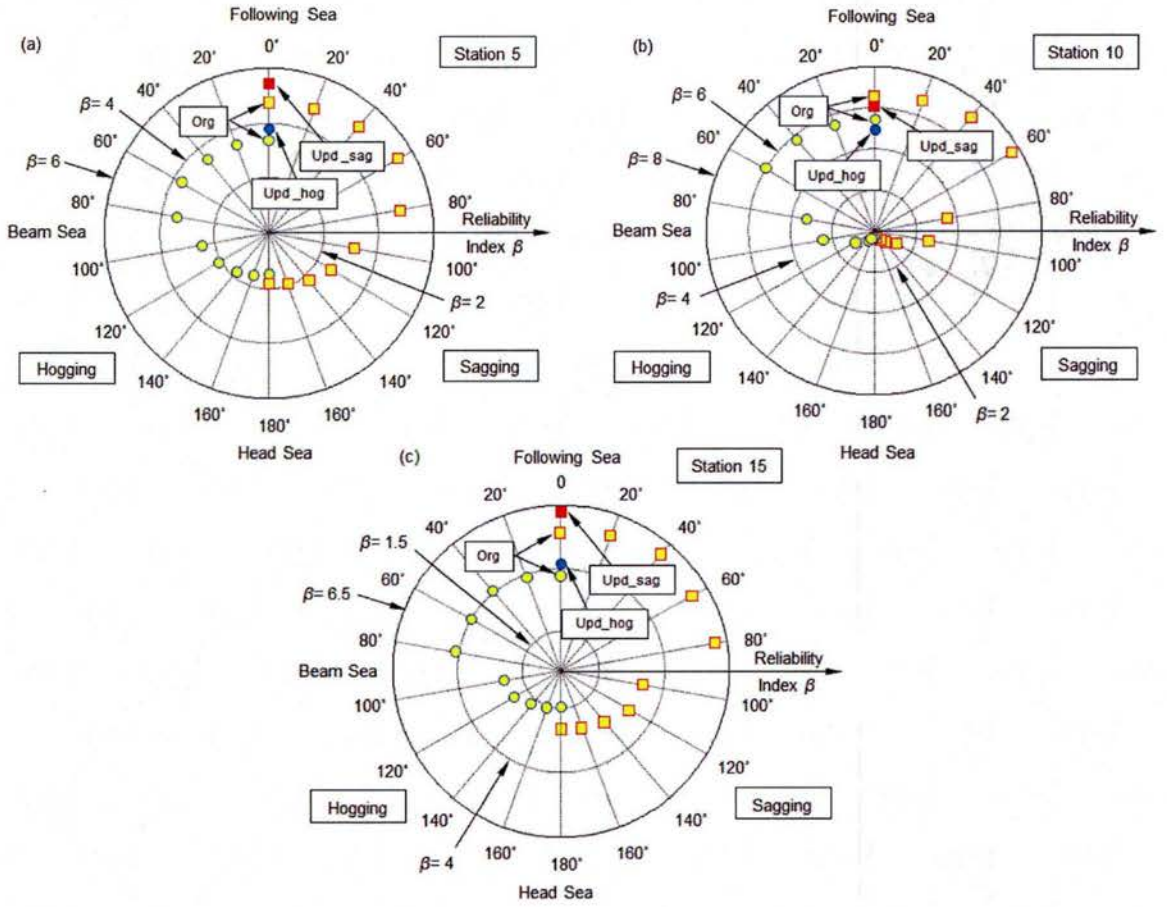

Figure 8 Polar representation of the original (denoted as "Org") and updated hogging (denoted as "Upd_hog") and sagging (denoted as "Upd_sag") reliability index (β) of: (a) Station 5; (b) Station 10; and (c) Station 15.

2.3. Conclusions

An approach for improving the accuracy in the reliability and redundancy assessment of ship cross-sections by incorporating the objective SHM data related to the prior load effects has been presented. The vertical bending moments associated with the ultimate and first failure for a given cross-section are evaluated using an optimization-based method and the progressive collapse method, respectively. The prior information on the wave-induced load effects is calculated based on the linear theory. Bayesian updating is then performed to update the prior load effects using the hogging and sagging peaks extracted from the processed SHM data. The original and updated reliability and redundancy indexes of the ship cross-sections are evaluated and the results are presented in polar plots. The following conclusions are drawn:

1. For a given sea state and ship speed, plotting the cross-section performance indicators in the polar coordinate system provides a straightforward representation of the effects of heading angle on the structural safety.
2. The cross-section reliability indexes associated with sagging are larger than those associated with hogging for all heading angles. However, a similar conclusion cannot be obtained for the cross-section redundancy. For the investigated JHSS in the operational case of sea state 7 and ship speed of 35 knots, the lowest reliability and redundancy indexes associated with the three stations occur at the heading angle of 180° for both hogging and sagging cases.
3. Integration of the SHM data can significantly reduce the uncertainty in a distribution parameter so that the updated performance indicators are closer to their true values. For the analyzed JHSS, the distribution types of the parameters α of three stations remain the same after updating while the mean values and standard deviations of α change. Therefore, the reliability and redundancy indexes associated with the three stations at the heading angle 0° are changed although the differences before and after updating are slight.
4. In this report, only the performance indicators at the heading angle of 0° are updated due to lack of the SHM data. However, if the SHM information associated with different operational conditions is available, the proposed approach can be used to update the entire reliability / redundancy polar plots of different sea states and ship velocities. For a given sea state that a ship might encounter during a journey, the ship operator can use these updated polar plots as a guidance to adjust the speed and heading angle to maintain the performance indicators above the defined thresholds.

3. Performance Assessment of Ship Hulls under Progressive and Sudden Damage

Performance assessment of damaged ship hull structures is crucial for informed-decision making after an accident. Grounding and collision are the most common accidents resulting in destruction of ships (Khan and Das, 2008). Evaluation and prediction of ship performance involve uncertainties due to the randomness in the material properties, the deterioration processes under the aggressive environmental conditions, and the imperfections in our engineering models. Nevertheless, these uncertainties should be treated properly in order to assess the performance of damaged ships. Reducing risk associated with loss of ship due to a post-accident collapse or disintegration of the hull during tow or rescue operations are of vital importance.

Research on performance assessment of damaged ships has attracted significant interest in the last two decades. Vertical bending moment capacity at critical sections has been the major performance indicator investigated. Wang et al. (2002a) provided a review of the state-of-the-art research on ship collision and grounding focusing on the definition of accident scenarios, evaluation approaches and acceptance criteria. Wang et al. (2002b) proposed an analytical

expression for assessing the residual strength of hull girders with damage and provided simple equations correlating residual strength with damage extent. Hussein and Guedes Soares (2009) studied the residual strength and reliability of double hull tankers for different damage scenarios.

The availability of information on the residual strength of a damaged hull structure can be very helpful for making decisions on how to proceed with the damaged ships after accidents. Moreover, the decision making process could be enhanced greatly when the information regarding the reliability of damaged ship hulls after grounding and collision is available. It is necessary to establish methods for reliability assessment of damaged ships for different operational conditions. For instance, the reliability information for different ship speeds, heading angles and sea states could provide guidance to avoid the ultimate failure of the damaged hull structures. In addition, the aging effects should be integrated in this approach.

In this research work, the probabilistic framework presented in Saydam and Frangopol (2013), for performance assessment of ship hulls under sudden damage accounting for different operational conditions is briefly discussed. Grounding and collision accidents are considered as sudden damage scenarios. The combined effects of sudden damage and progressive deterioration due to corrosion are investigated. The reliability index and a probabilistic robustness index are selected as the performance indicators to account for the uncertainties. The longitudinal bending moment failure is considered as the limit state. The longitudinal bending moment capacity of the intact and damaged ship hulls is assessed using an optimization-based version of incremental curvature method. The approach is illustrated on an oil tanker. In addition, aging effects on ship reliability are investigated.

3.1. Grounding and Collision Damage

Performance assessment of damaged ships includes identifying accident scenarios, estimating the probability of occurrence of different accidents, reliability analysis of the structure under the accident scenarios, and evaluating the consequences of structural damage and failure. This investigation primarily focuses on the reliability analysis under various damage scenarios associated with grounding and collision. The extent of the damage on the ship hull after grounding and collision accidents depends on several parameters such as the speed at contact, contact angle, and mechanical properties of the structures in contact, among others. In grounding and collision damage scenarios, it is assumed that the damaged part of the hull is unable to carry longitudinal stresses and is excluded from the ultimate bending moment computations.

Grounding with a forward speed on a rocky sea bed may result in considerable rupture of the bottom of the hull structure. The damage should be assumed to be located unfavorably anywhere on the flat bottom. ABS guidelines (1995) consider the damage to be within the fore part of the hull between 0.5 L and 0.2 L aft from forward perpendicular, where L is the length of the ship. The width of the damage is assumed to be the greater of 4 m or B/6 (i.e., one sixth of breadth B).

According to ABS (1995), the damaged members are excluded from the hull girder section modulus calculation.

A collision with another ship on one side may result in extensive rupture of the side of the hull structure. ABS guidelines (1995) assume that the damage is in the most unfavorable location anywhere between 0.15 L aft from the forward perpendicular and 0.2 L forward from the aft perpendicular. The collision damage is assumed to be located at upper part of the side shell, down from the stringer plate of the strength deck. The shell plating for vertical extent of the greater of 4 m or D/4 (i.e., one fourth of the depth D) and the attached girders and side longitudinals are supposed to be excluded from the capacity analysis.

3.2. Methodology for Performance Assessment of Damaged Ship Hulls

Based on Saydam and Frangopol (2013), the methodology for assessing the performance of damaged ship hull considering aging effects is illustrated in Figure 9. The first step of the methodology is identifying the failure mode to investigate. In general, longitudinal bending moment failure at the mid-section of the ship hull is considered as the limit state. The next steps can be basically categorized in two parts. These are the computations for resistance and loads. The random variables associated with the resistance must be identified. The hull capacity associated with this failure mode should be computed considering uncertainties for the intact and damaged (sudden damage) hull associated with the selected grounding and collision damage scenarios. One component of the load effects is due to the still water. The load effects produced by the still water can be subjected to change as the effect of sudden damage to the ship increases and the load distribution over the length changes.

The approach proposed in Okasha and Frangopol (2010) and further extended in Decò et al. (2011, 2012) is used to quantify the ship resistance while the loading estimation model presented earlier in this report is adopted to compute the load effects. Using a software program capable of performing first order reliability method (FORM) or second order reliability method (SORM), the instantaneous reliability index associated with one sudden damage scenario, one operational condition, and at a point in time can be computed. In order to obtain, time-variation of the reliability the procedure should be repeated with time-variant values of hull capacity as it is reducing in time due to the effects of corrosion. The effects of different levels of still water loads on reliability can be investigated by repeating the procedure for different values of still water load effects. Furthermore, the procedure should be repeated for different operational conditions to obtain the reliability index with respect to speed, heading and sea state.

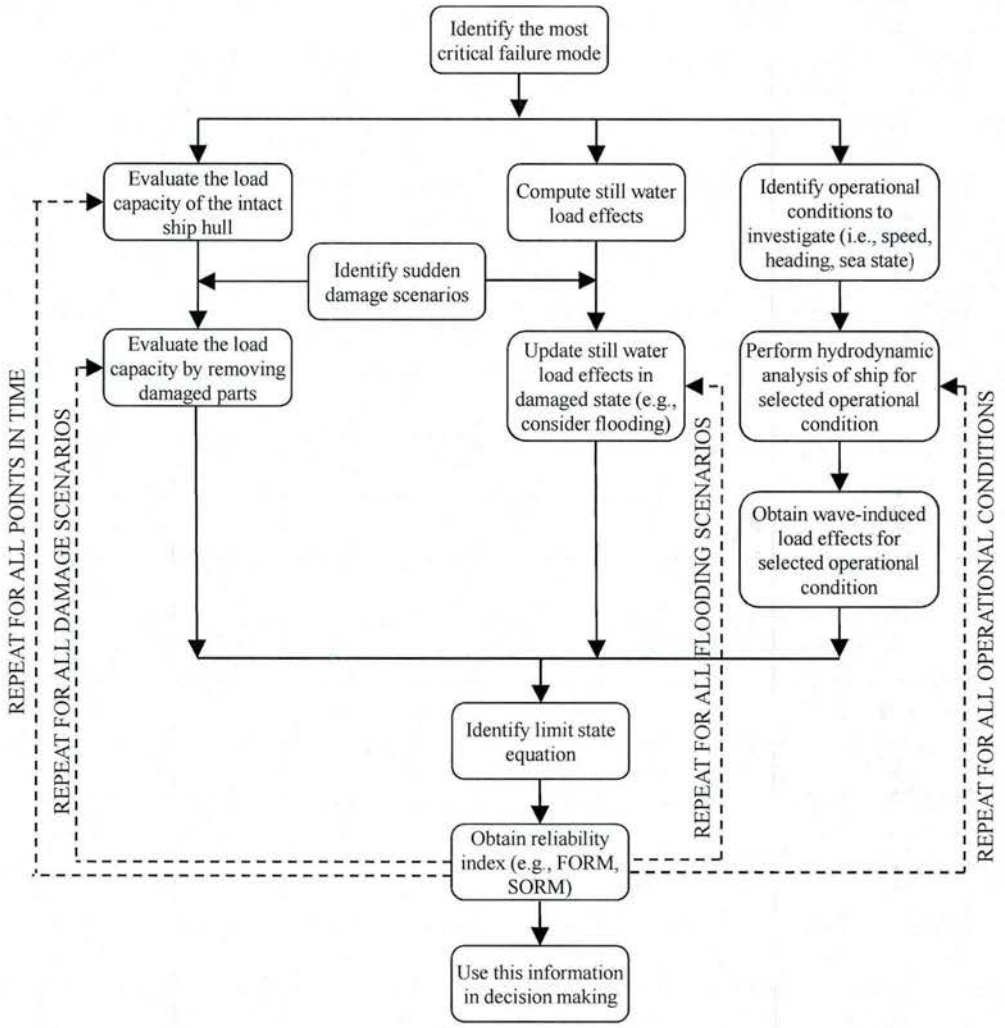

Figure 9 Methodology of assessing time-variant performance of damaged ship hulls

In this research work, the safety evaluation of intact and damaged hull structures is based on reliability theory. The limit states associated with the flexural failure of the hull girder at mid-section and discussed in the previous section are adopted. In addition to the reliability index, several performance indicators are investigated. The residual strength factor provides a measure for the strength of the system in a damaged condition compared to the intact system. It is defined as the ratio of the capacity of the damaged structure or element to the capacity of the intact structure (Frangopol and Curley, 1987). In this approach, the residual strength factor for each damage scenario R_i is formulated as

$$RSF_i = \frac{\mathrm{E}(MC_i)}{\mathrm{E}(MC_0)} \tag{26}$$

where E(MC_i) and E(MC_0) are the mean values of the vertical bending moment capacity of the damaged and intact hull, respectively. Residual strength factor takes values between 0, when damaged structure has zero capacity, and 1.0, when damaged structure does not have any reduction in load-carrying capacity.

Another performance indicator investigated is used to quantify the robustness of the ship hull in a probabilistic manner. A measure of robustness is formulated as

$$RI_i = \frac{\beta_i}{\beta_0} \tag{27}$$

where RI_i is the robustness index for associated with damage scenario i, and β_i and β_0 are the reliability indices associated with the damaged and intact hull, respectively.

3.3. Illustrative Example

The proposed methodology is illustrated on a hull structure which was analyzed by Akpan et al. (2002). The length of the ship L is 220 m, breadth B is 38.1 m, height H is 17.4 m, block coefficient C_b is 0.75, the elastic modulus E is 208 MPa, the deck and keel yielding stress σ_{Yp} is 315 MPa, and the side panels yielding stress σ_{Ys} is 281 MPa. The cross-section of the mid-ship is shown in Figure 10.

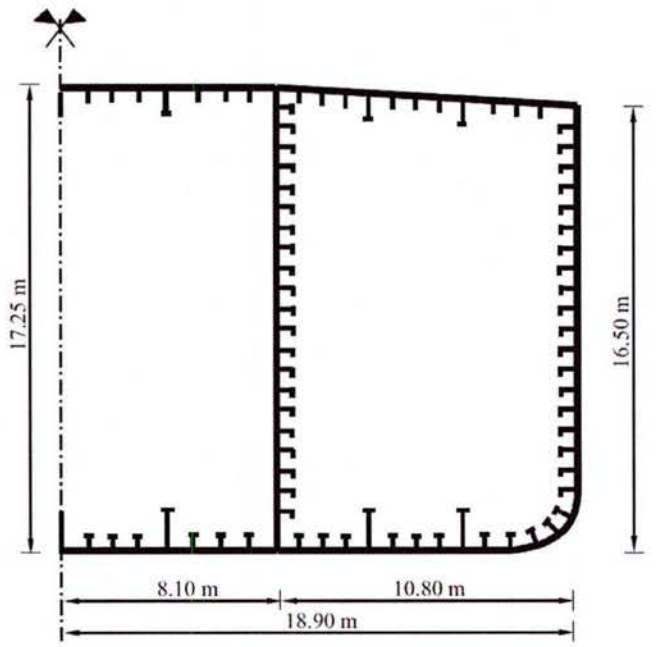

Figure 10 Mid-section dimensions of the investigated ship and its six type of stiffeners (adapted from Akpan et al. 2002)

3.3.1. Sudden Damage Scenarios

In order to investigate the residual strength and performance of the damaged hull, six sudden damaged scenarios are considered. The first three are grounding damage scenarios. In these scenarios, a part of the bottom of the hull is assumed to be damaged with an extent proportional to the ship breadth B. The considered damage extents are $B/6$, $B/3$, and $B/2$, the smallest one being the damage extent suggested by ABS (1995). The center of the damaged part is assumed to coincide with the symmetry line of the hull section. The three grounding damage scenarios are illustrated in Figure 11(a), (b), and (c). The remaining three are collision damage scenarios (Figure 11(d), (e), and (f)). In these scenarios, a part of the side hull is assumed to be damaged with an extent proportional to the depth of the ship (D). The considered damage extents are $D/4$, $D/3$, and $D/2$, the smallest one being the damage extend suggested by ABS (1995). The damage is assumed to start from the top of the side hull and extent downwards.

3.3.2. Resistance and Residual Strength Factor

The hull flexural strength is evaluated based on the method by Okasha and Frangopol (2010) described previously. Load effects are calculated based on the model adopted in Decò et al. 2012 and presented above. The random variables and their associated parameters are described in details in Saydam and Frangopol (2013).

The mean vertical bending moment capacity of the hull with respect to ship age for different sudden damage scenarios and the hull with no sudden damage is presented in Figure 12(a) and (b) for sagging and hogging, respectively. The strength of the hull in hogging is slightly higher than that in sagging. Among the damaged scenarios, the last two grounding damage scenarios DS 2 and DS 3 result in the largest reduction in the ship hull. The first collision damage scenario DS 4 has almost no effect on the vertical bending moment capacity of the structure. In Figure 12(a), Curve A represents the mean vertical bending moment capacity profile for sagging if sudden damage scenario DS 3 occurs at $t = 10$ years and no repair action is taken afterwards. The sudden drop at $t = 10$ years is the result of the sudden damage and the progressive reduction is due to corrosion. Similarly, Curve B represents the mean vertical bending moment capacity profile for sagging if sudden damage scenario DS 6 occurs at $t = 15$ years. In Figure 12(b), Curve C represents the mean vertical bending moment capacity profile for hogging if sudden damage scenario DS 2 occurs at $t = 25$ years.

Residual strength factors indicate the remaining percentage of the bending moment capacity. The time-variation of residual strength factors for different sudden damage scenarios is presented in Figure 13(a) and (b) for sagging and hogging, respectively. DS 4 and DS 1 yield the highest residual strength factors in sagging while DS 4 and DS 5 yield the highest residual strength factors in hogging. The lowest residual strength factors belong to DS 3 and DS 2 both in sagging and hogging. These factors are decreasing in time due to the effects of corrosion.

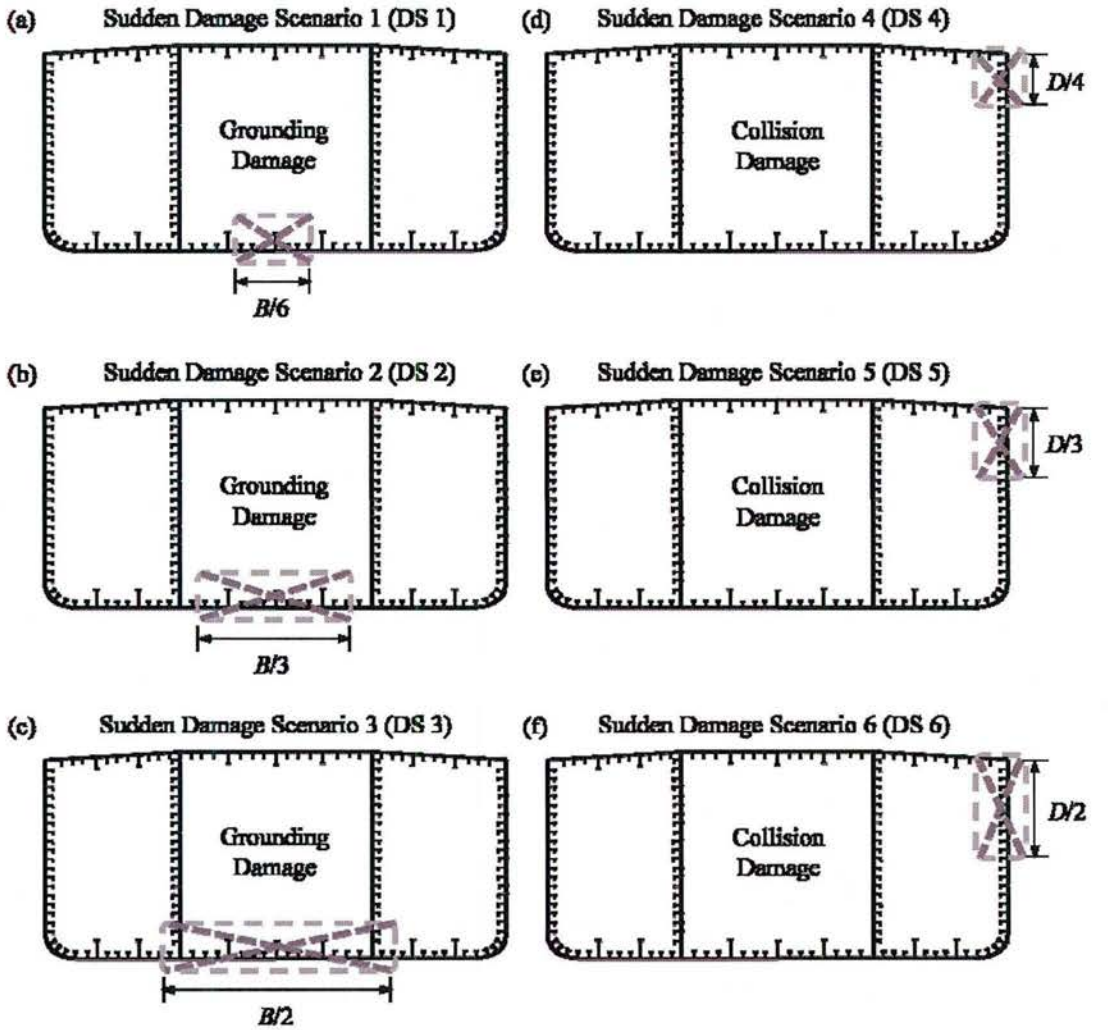

Figure 11 Sudden damage scenarios investigated

3.3.3. *Reliability*

The reliability of the intact and damaged ship hull is evaluated in time for various operational conditions. Ship structural performance is evaluated for different ship headings. Angles between 0° (following sea) and 180° (head sea) by increments of 15° are considered. Wind sea accounting for sea states 5, 6, and 7 (SS 5, SS 6, and SS 7) is included in the analysis. The reliability analyses are conducted based on FORM and the limit states defined in the previous section using reliability software RELSYS (Estes and Frangopol 1998). In Figure 14(a), the variation of the reliability index β with respect to heading angle for sudden damage scenarios DS 1, DS 2, and DS 3 with constant sea state 5, ship speed $U = 10$ knots, and time $t = 0$ is presented. At $t = 0$, the structure is intact of corrosion (there is no section loss in structural members), however, the

effects of accidental scenarios are illustrated for this initial time instant. The lowest reliability index with respect to heading angle is obtained at 180° and the highest one is obtained at 90°.

The reliability indices in hogging are less than those in sagging. DS 1 causes a very slight reduction in reliability index while DS 2 and DS 3 reduce the reliability index, by around 0.5 and 0.6, respectively. In Figure 14(b), the variation of the reliability index with respect to heading angle for sudden damage scenarios DS 4, DS 5, and DS 6 with constant sea state 5, ship speed U = 10 knots, and time t = 0 is presented. The lowest reliability index with respect to heading angle is obtained at 180° and the highest at 90°.

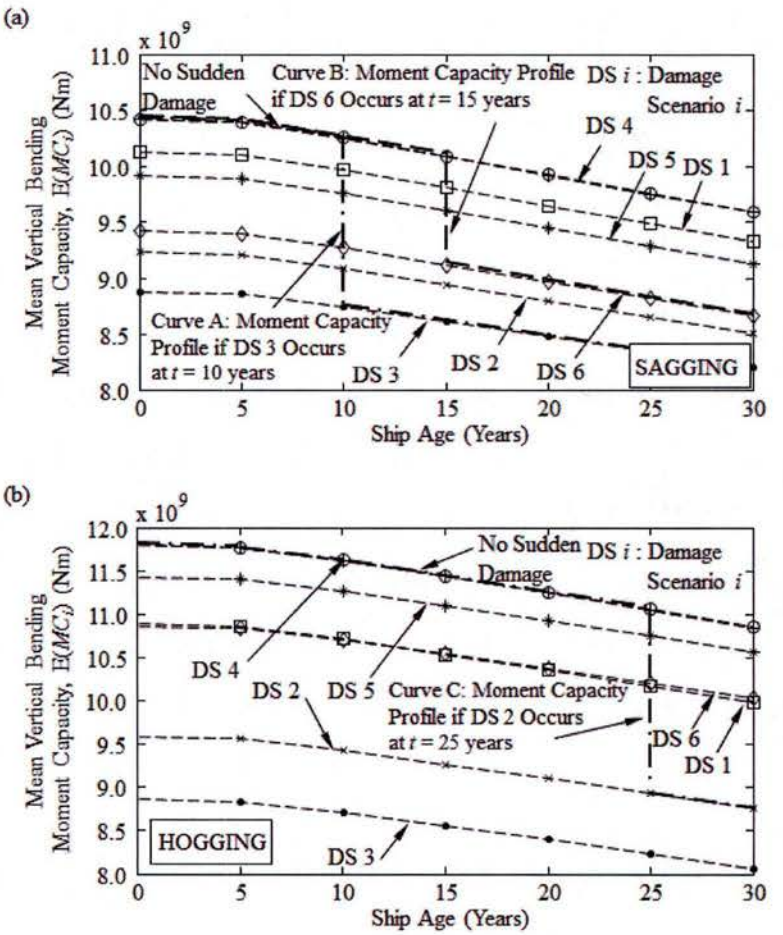

Figure 12 Variation of mean bending capacity of mid-ship for the six different sudden damage scenarios shown in Figure 11, (a) sagging and (b) hogging

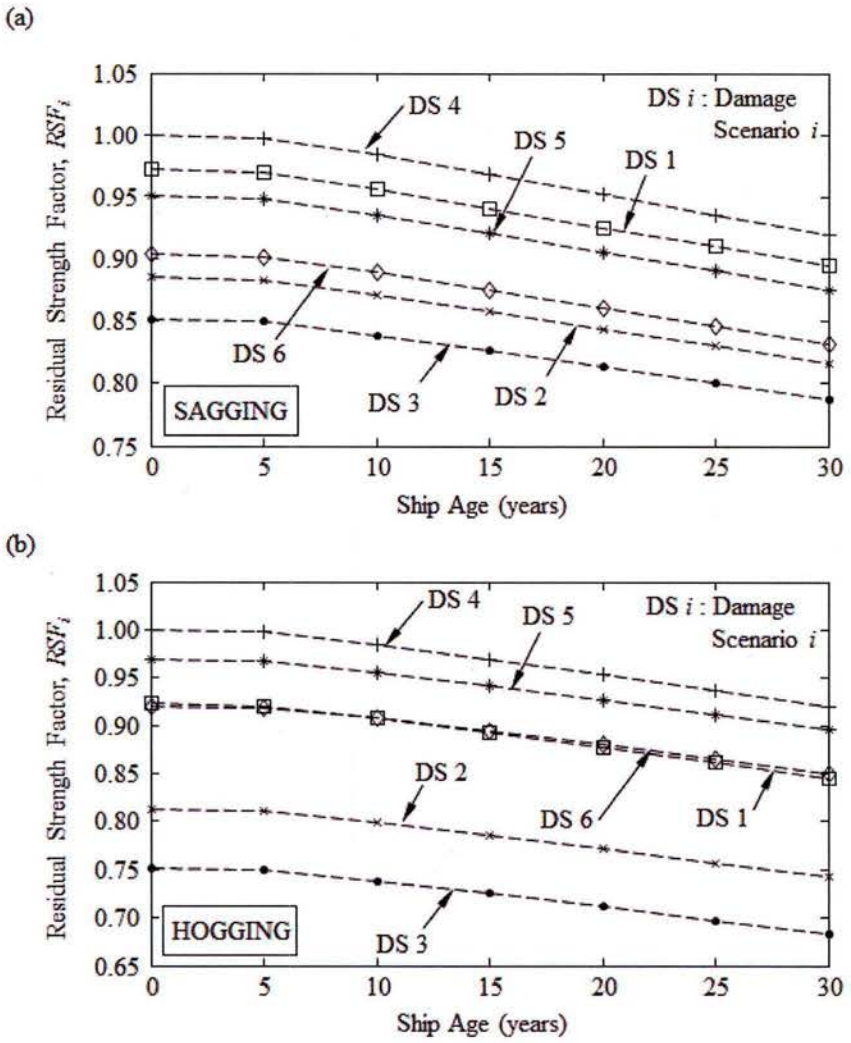

Figure 13 Variation of residual strength for the six different sudden damage scenarios shown in Figure 11, (a) sagging and (b) hogging

The reliability indices in hogging are less than those in sagging. DS 4 does not cause a reduction in reliability index at all; however, DS 5 and DS 6 reduce the reliability index by around 0.2 and 0.4, respectively. These results indicate that the contribution of the bottom shell to the bending reliability is very significant. Similarly, the effect of the sea state and the ship state on the reliability for a given damage scenario can be found.

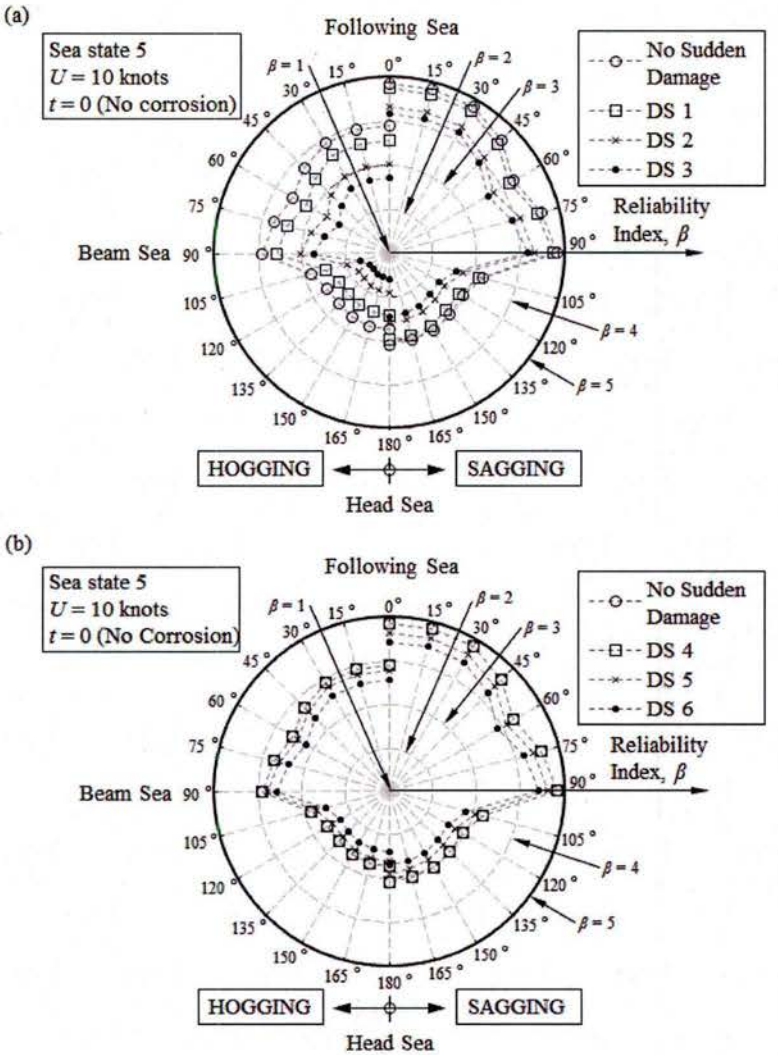

Figure 14 Variation of reliability index with respect to heading angle for sea state 5, ship speed U = 10 knots, time t = 0, (a) sudden damage scenarios 1, 2, and 3 and (b) sudden damage scenarios 4, 5, and 6

The results explained above do not consider the effects of flooding after sudden damage. Hussein and Goades Soares (2009) showed that the still water bending moment is increased with flooding. In this report, the effect of flooding is investigated by increasing the still water bending moment by 25% and 50%. In Figure 15(a), the variation of the reliability index with respect to the heading angle and still water bending moment for DS 2 under constant sea state 5, ship speed U = 0 knots, and time t = 0 is presented. Increase in still water bending moment reduces the reliability significantly. At 0° heading angle, 25% increase in still water bending moment reduces the reliability index by 0.9 while 50% increase in still water bending moment reduces the reliability index by 1.5. In Figure 15(b), the variation of the reliability index with respect to the

heading angle and time for DS 4 with constant sea state 5 and ship speed U = 0 knots is presented. The results indicate that the corrosion causes significant reduction in safety in long term if proper maintenance actions are not taken.

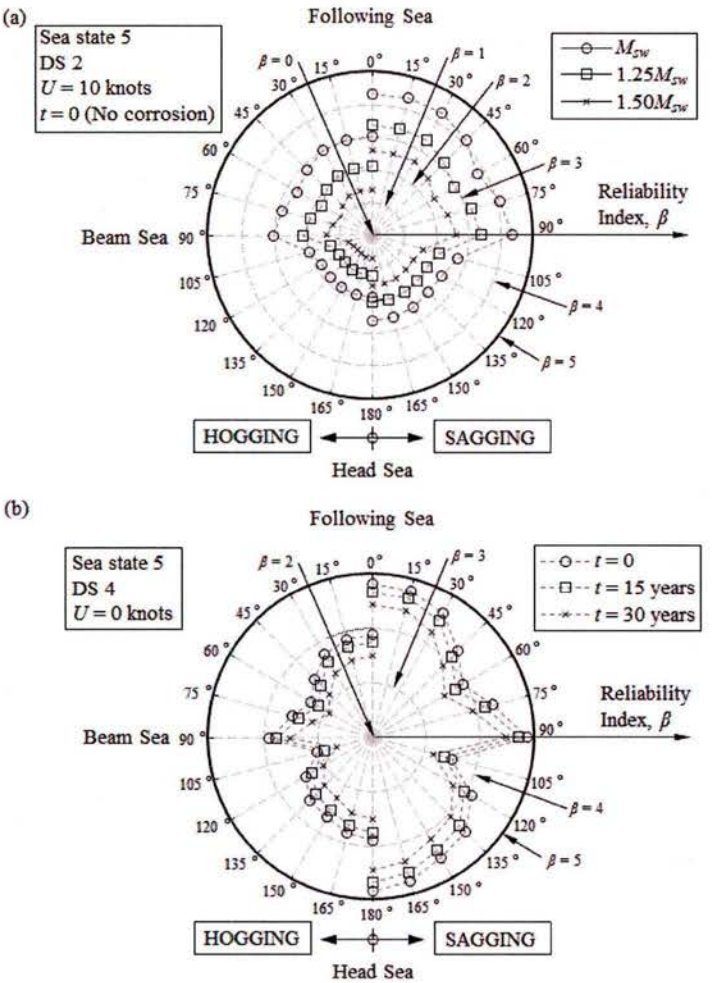

Figure 15 Variation of reliability index with respect to heading angle for (a) different values of still water bending moment and (b) different points in time

3.3.4. Robustness Index

The robustness for the sudden damage scenarios is evaluated based on Eq. (27). In the cases mentioned below, β_0 is taken as the highest reliability index of the hull with no sudden damage with respect to heading angle. In Figure 16(a), the variation of the robustness index with respect to heading angle for sudden damage scenarios DS 1, DS 2, and DS 3 with constant sea state 5, ship speed U = 10 knots, and time t = 0 is presented. The lowest robustness index with respect to

heading angle is obtained at 180° and the highest one is obtained at 90°. The robustness indices in hogging are less than those in sagging. DS 3 yields the lowest robustness index, which means that is it is the most severe scenario. In Figure 16(b), the variation of the robustness index with respect to the heading angle and time for DS 4 with constant sea state 5 and ship speed $U = 0$ knots is presented.

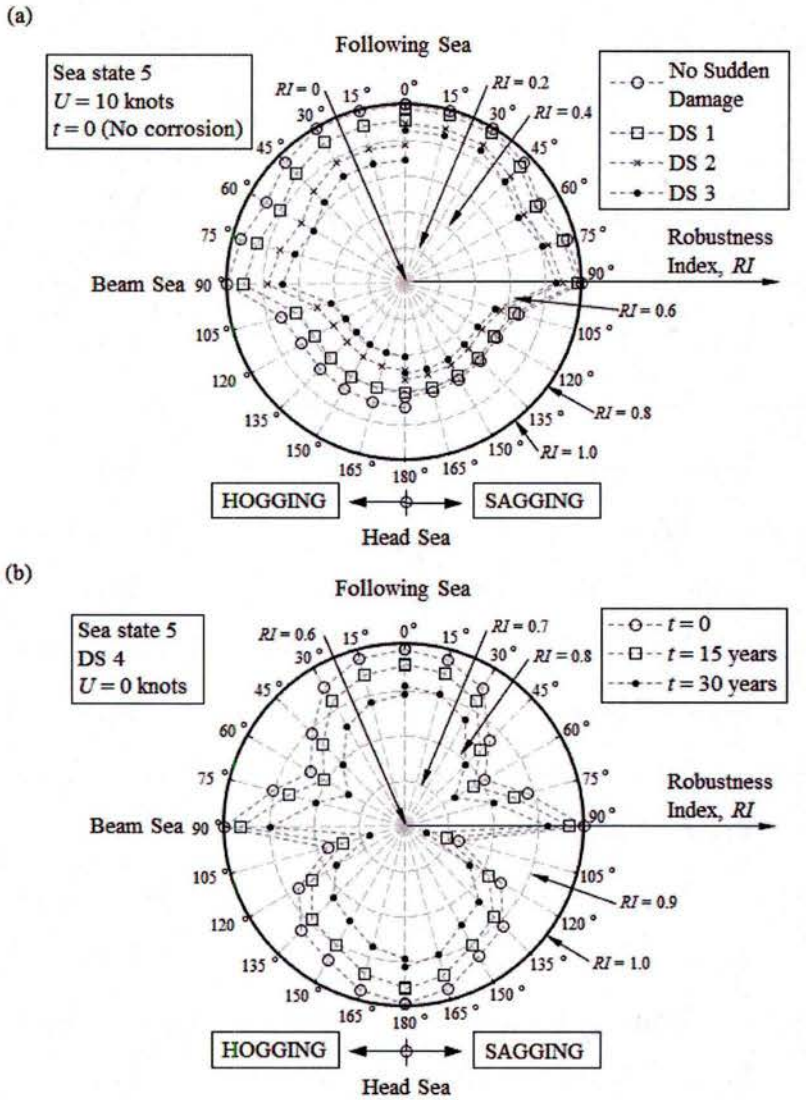

Figure 16 Variation of robustness index with respect to heading angle for (a) different sudden damage scenarios, and (b) different points in time

3.4. Conclusions

In this subsection, a framework for performance assessment of damaged ship hulls under different operational conditions considering grounding and collision accidents as sudden damage is presented. The combined effects of sudden damage and aging on ship performance are investigated. The performance of ship hull is quantified in terms of several performance indicators. The approach is illustrated on an oil tanker.

The following conclusions are drawn.

1. After accidents, ultimate failure of ships may occur depending on the extent of the damage. The outlined methodology can be very helpful in decision making on how to deal with damaged ship by providing information on the reliability of the damaged ship under different operational conditions. The methodology can be used to investigate the effects of ship damage scenarios occurring at different points in the service life.
2. Residual strength factor can be used time effectively to quantify the loss of hull strength under different scenarios and comparison. The results show that corrosion can have significant impact on the residual strength of ships. Time effects should be included in the reliability, redundancy, and robustness of aging ships.
3. The performance of damaged ships can be evaluated in a probabilistic manner. The results indicate that operational conditions have very significant effects on reliability. Reliability for different operational conditions has to be evaluated for damage scenarios. Reliability of a ship highly depends on speed, heading angle, sea state, age of the ship and damage condition. Corrosion may cause significant reduction in reliability. The reliability information of a damaged ship under different operational conditions considering time effects is very important, during tow or rescue operations. For instance, the ship speed could be adjusted so that the reliability of the damaged ship remains above a predefined threshold.
4. The robustness index is useful for comparison of the severity of sudden damage scenarios. Compared to the residual strength factor, it contains additional information as it is based on reliability index rather than the mean hull strength.
5. Some operational conditions result in significant reduction in the performance. In general, the worst performance is obtained under head sea. The effect of the sea state becomes more dominant when ship speed is increasing.
6. The proposed methodology can be effectively used when combined with the real time structural health monitoring tools. The information obtained from different critical locations of the ship in real time will give the possibility to adjust the operational condition to keep the integrity of a damaged ship.

The proposed framework is aimed to be used in optimization of the design and maintenance of ships and actions after ship accidents. In this report, the effects of different sudden damage scenarios are investigated separately. Further research on this topic should include a methodology for combining the effects of different scenarios in one performance indicator. This is very useful for direct comparison of alternatives in decision making.

4. Incorporation of Structural Health Monitoring Data to Compute the Fatigue Reliability and Service Life of Aluminum Vessels

The evolution of naval vessels toward high-speed crafts subjected to severe sea conditions has promoted an increasing interest in lightweight high-strength materials. Due to its strength and weight characteristics, aluminum has been proven especially suitable as construction material for hull structures as well as other vessel parts. However, fatigue in aluminum naval crafts needs to be effectively addressed for the proper life-cycle assessment. Structural health monitoring systems constitute effective tools for measuring the structural response and assessing the structural performance under actual operational conditions. In this subsection, an approach for using structural health monitoring information in the fatigue reliability analysis and service life prediction of aluminum naval vessels is presented. The accumulated fatigue damage and the fatigue reliability are quantified based on structural health monitoring data acquired under different operational conditions, specified by the ship speeds, sea states, and heading angles. Additionally, an approach for estimating the reliability-based fatigue life under a given operational profile is presented. Seakeeping trial data of an aluminum high-speed naval vessel are used to illustrate the proposed approach.

4.1. Fatigue Reliability

Ship structures are naturally subjected to variable amplitude stress cycles. If the distribution of the stress cycle amplitudes is known, Miner's damage accumulation rule (Miner 1945) can be used to find a representative equivalent constant amplitude stress range. By considering the stress cycle amplitude histogram, and under the assumption of linear damage accumulation, Miner's damage accumulation index D is the defined as

$$D = \sum_{i=1}^{n_{ss}} \frac{n_i}{N_i} \tag{28}$$

where n_{ss} = number of stress range bins in a stress-range histogram, n_i = number of stress cycles in the ith bin with stress range S_i and N_i = number of cycles to failure under the stress range S_i. According to Miner's damage accumulation rule, the failure of the detail occurs when D = 1.0. The equivalent stress range can be computed as using the probability density function $f_S(s)$ of the stress range S as follows

$$S_{re} = \left[\int_0^{\infty} s^m \cdot f_S(s) \cdot ds \right]^{\frac{1}{m}} \tag{29}$$

For an equivalent constant amplitude stress range, fatigue life can be measured as the number of cycles to failure. This number of cycles N, in conjunction with the average annual number of cycles N_{avg} obtained by the SHM data, returns an estimation of the fatigue life t_f in years, using the following equation

$$t_f = \frac{N}{N_{avg}} \tag{30}$$

For the probabilistic assessment of the remaining fatigue life, a reliability approach can be used based on the definition of the following performance function

$$g(t) = \Delta - D(t) \tag{31}$$

where Δ = Miner's critical damage accumulation index, indicating the allowable accumulated damage and assumed lognormal distributed with mean 1.0 and coefficient of variation (COV) 0.48 (Collette and Incecik 2006); $D(t)$ = Miner's damage accumulation index, which can be expressed as

$$D(t) = \frac{N(t)}{A} \cdot S_{re}^m = \frac{t \cdot N_{avg}}{A} \cdot S_{re}^m \tag{32}$$

where A and m = S-N relationship parameters, S_{re} = equivalent constant amplitude stress range, and N_{avg} = average annual number of cycles.

4.2. Fatigue Reliability under Multiple Operational Conditions

When SHM is available, the short-term response of the ship detail, for a selected operational condition, can be directly found using strain measurements recorded during seakeeping trials, performed on the vessel at the beginning of its service life. Subsequently, for a prescribed operational profile with assigned probabilities of occurrence p_j of different sea states, speeds, and heading angles, the total damage accumulation index D_T can be found, under the assumption of linear damage accumulation, as

$$D_T = T_r \cdot \sum_{j=1}^{n_o} p_j \cdot D_j \tag{33}$$

where n_o = number of operational conditions encountered by the ship during the reference time T_r (years), and D_j = annual damage accumulation index for the detail associated with the jth operational condition. Finally, the fatigue life T_f can be found as

$$T_f = \frac{T_r}{D_T} = \frac{1}{\sum_{j=1}^{n_o} p_j \cdot D_j} \tag{34}$$

Similarly, the fatigue reliability under multiple operational conditions can be evaluated using the performance function

$$g(t) = \Delta - D_T \tag{35}$$

which can be expressed as

$$g(t) = \Delta - T_r \cdot \sum_{j=1}^{n_o} p_j \cdot D_j \tag{36}$$

the performance function can be rewritten as

$$g(t) = \Delta - T_r \cdot \sum_{j=1}^{n_o} p_j \cdot N_{avg_j} \cdot \frac{S_{re_j}^m}{A} \tag{37}$$

where N_{avg_j} = average number of cycles acting on the detail during one year of exposure to the *j*th operational condition, and S_{re_j} = constant equivalent stress range acting on the detail at the *j*th operational condition. The stress range and the number of cycles can be found using the SHM data collected during the water trials.

4.3. Illustrative Example

The fatigue assessment and reliability analysis presented in this paper are applied to the HSV-2 swift, an aluminum wave piercing catamaran, with an overall length of 98 meters, designed and built in Tasmania, Australia. As indicated in [38], a total of 16 sensors were placed for measuring the structural response due to global loading. These sensors, denoted as T1-1 to T1-16, recorded the global bending stresses, pitch connecting moments, and split responses. Another group of sensors, T2-1 to T2-9 and T2-12 to T2-21, was installed to measure the stress concentration at various locations. Positions of the structural response sensors (i.e., T1 and T2 sensors) were selected based on detailed finite element analysis and previous experience with similar vessels (Brady 2004b). Data recorded by these sensors have a sample rate of 100 Hz. Seakeeping trials were set up to expose the ship to different operational conditions covering multiple speeds, wave headings, and sea states. Thus, the trials were performed by executing octagon patterns where wave headings of 0°, 45°, 90°, 135°, 180°, 225°, 270°, 315°, and 360° were encountered. However, considering the symmetry of the vessel, most of the runs were executed to cover only 5 heading angles. A total of 22 trial octagons have been performed at different speeds ranging between 2 and 35 knots at sea states 4 and 5. To study the effect of the ride control system on the structural response, a portion of those trial octagons was performed with the T-foil deployed while the rest was performed with the T-foil retracted. Slam load analysis performed by Brady (2004a) showed that deploying the T-foil may slightly increase the slam pressure; however, it reduces the rate of slams. The study by Brady (2004a) was based on a comparison at speed 20 knots with no assessment with respect to fatigue, which is sensitive to both the pressures and the number of cycles. In this paper, a comparison of the fatigue response with respect to the T-foil deployment is performed at different operational conditions.

4.3.1. *Fatigue Analysis*

For fatigue analysis, the T2 strain gages are used with the hot spot structural stress S-N approach. Among those sensors, the sensor T2-4, placed to measure the bending response on keel frame 26 on the port side, is analyzed herein. Fatigue damage assessment is performed on the detail equipped with the sensor T2-4 using the strain measurements for the range of available operational conditions. This task is performed considering an annual ship operation rate $o_r = 2/3$ (i.e. it is considered that the ship is operated 2/3 of the time). The results of such analysis provide indications on the effect of different operational conditions on the fatigue damage. Figure 17(a) shows the annual damage accumulation with respect to the speed for sea states 4 and 5. It should be noted that the strain records of the operational condition at sea state 5 with speed of 20 knots and heading angle 0^o were not included in the monitoring data. As expected, the damage accumulation increases with the speed. Higher sea states have significant effect on the damage accumulation especially at speeds higher than 30 knots. At 35 knots, an increase of 250% in the damage accumulation is found when the sea state changes from 4 to 5. Additionally, the study is performed with respect to the significant wave height and the encountered wave period, which is dependent on the ship speed. The results reported in Figure 17(b) illustrate the variation in the annual fatigue damage accumulation of the detail with respect to the encountered wave period for different values of the significant wave height *H*. As shown, the damage accumulation decreases with the increase in the encountered wave period. Additionally, the accumulation increases with the increase in the significant wave height H; this effect is amplified for low values of the encountered wave period (i.e. at higher navigation speeds). It is also observed that the difference in the damage accumulation occurring at sea state 4 for speeds of 20 and 30 knots is very small. This can be attributed to the difference in the wave period between the two operational conditions.

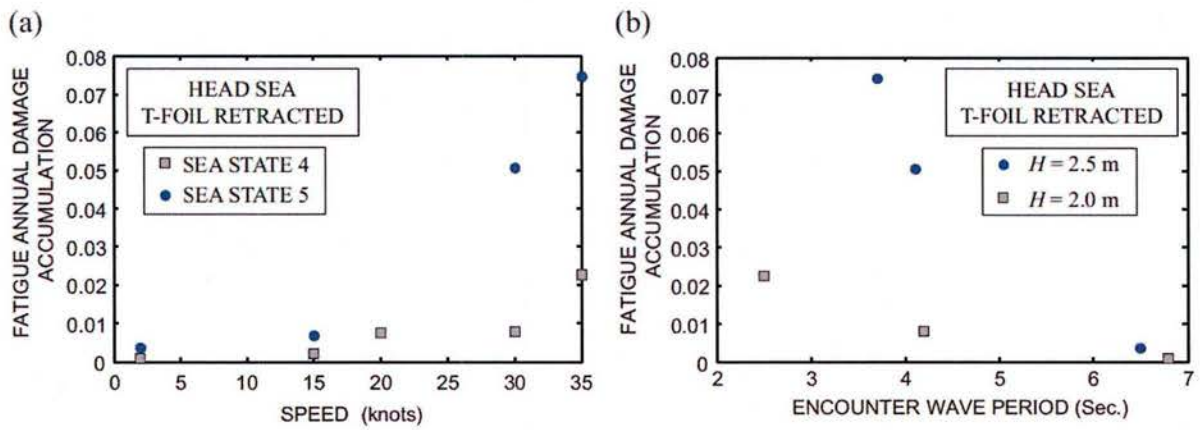

Figure 17. Variation in the annual fatigue damage accumulation of the detail with respect to (a) speed of the ship for different sea states and (b) encountered wave period for different values of the significant wave height *H*.

The effect of the T-foil deployment on the fatigue damage accumulation at various operational conditions has also been investigated. The results are depicted in Figure 18 for sea state 5 and head sea condition, considering various speeds, and T-foil deployed or retracted. At low speeds (15 knots and below), the effect of the T-foil on the damage accumulation seems negligible. However, with the increase in speed, a different behavior is observed; at 30 knots, the damage accumulation is lower with the T-foil retracted, with a reduction of 30% in the damage accumulation when compared to the case with the T-foil deployed, whereas at 35 knots, the T-foil deployment reduces the damage accumulation by about 30%. Therefore, with respect to the fatigue damage accumulation, the T-foil seems to be not effective at speeds 30, 15, and 2 knots.

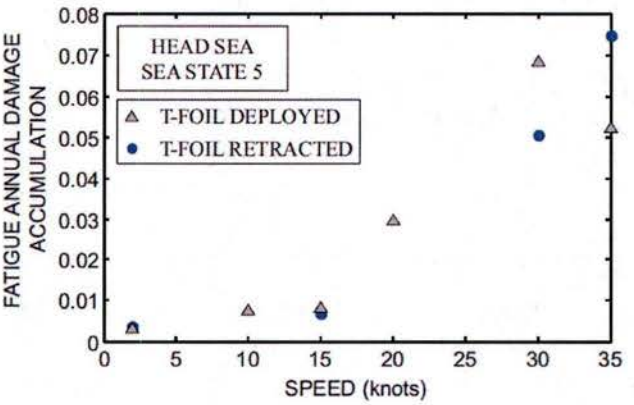

Figure 18 Variation in the annual fatigue damage accumulation of the detail with respect to the speed of the ship showing the effect of the T-foil deployment on the fatigue damage accumulation.

Figure 19(a) and (b) provide, in polar plot representation, the annual damage accumulation at speeds of 15 and 30 knots for sea states 4 and 5, respectively. As shown, the speed of the ship has a significant effect on the damage accumulation at different heading angles and sea states.

4.3.2. Fatigue Reliability

Fatigue reliability for the individual operational conditions is found by means of Equation (32) using the software CalREL (Liu et al. 1987) that implements second order reliability method (SORM). Fig. 13 plots the time-variant reliability index for different operational conditions, assuming that the ship is subjected to the same operational condition throughout its service life, with an annual operational rate o_r = 2/3. Figure 20(a) shows the reliability profiles at speed 30 knots for different sea states whereas Figure 20(b) highlights the effect of the speed on the fatigue reliability by showing the fatigue reliability profile for speeds 15, 20, 30, and 35 knots, at sea state 5. Figure 20(c) shows a comparison between the reliability profiles obtained with the T-foil deployed and retracted at speed 35 knots. As expected from previous results, using the T-foil improves the reliability at high speeds, increasing the predicted fatigue life by more than 100%, specifically, 28.1 years and 13.4 years for target reliability indices of 2.0 and 3.0, respectively.

The effect of the heading angle is shown in Figure 20(d) in which the reliability is plotted for 0°, 45° and 90° heading angles. For other heading angles, since the damage accumulation is significantly low, the resulting reliability profiles are extremely high compared to those associated with the considered angles; thus, these profiles have been excluded from the plot.

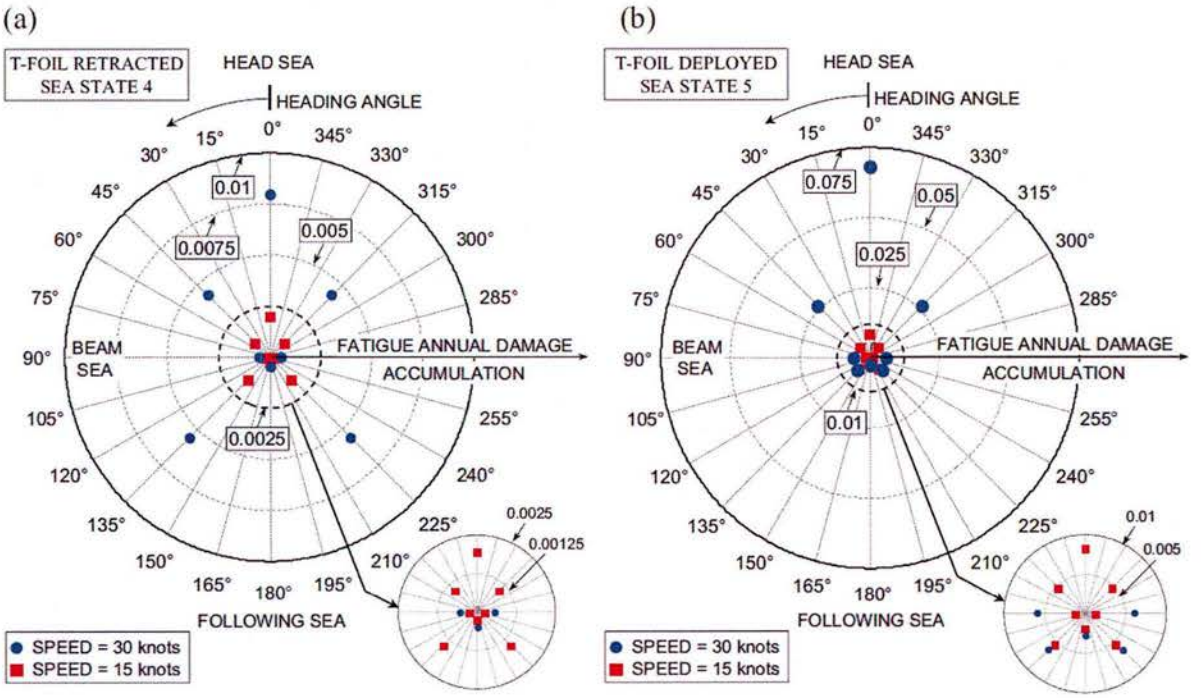

Figure 19 Comparison between the annual fatigue damage accumulation at speeds of 15 and 35 knots with respect to the heading angle for (a) sea state 4 with the T-foil retracted and (b) sea state 5 with the T-foil deployed.

When the real operational profile recorded in the ship log files is considered, a different reliability profile has to be expected. If the time spent in each operational condition or the probability of being in each operational condition is known, the overall fatigue reliability, as a result of being exposed to multiple operational states, can be found using Equation (37). This information, in conjunction with the SHM data recorded during the sea keeping trials at an early stage of the ship service life, can be used to project the long-term reliability profile of the ship. As an example, if a simple operational profile is provided where the probabilities of being in each sea state, heading angle, and speed are given for three different operational conditions (i.e., C1, C2 and C3). In this case, the reliability analysis is performed using the software CalREL. Figure 21 shows the reliability profiles of each operational condition, assuming complete operability of the ship in this condition, and the overall reliability profile arising from the real operability in the mixed operational states. The target service life can be easily estimated by establishing a reliability index threshold β_{target}. Setting $\beta_{target} = 2.0$ returns a fatigue life of 13.30 years at the detail, whereas, $\beta_{target} = 3.0$ gives 6.38 years of fatigue life.

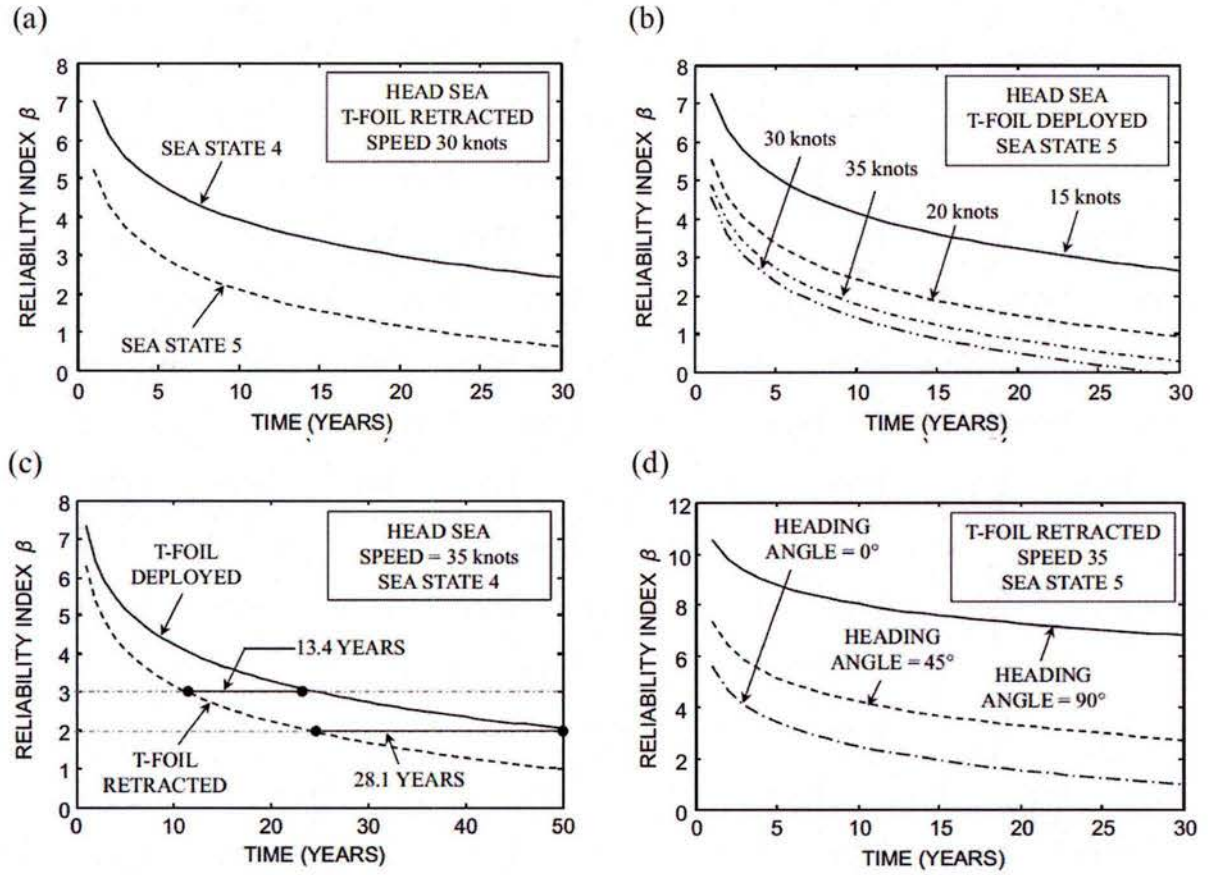

Figure 20 Time-variant fatigue reliability index and its sensitivity with respect to the effect of (a) sea states, (b) speeds, (c) T-foil deployment, and (d) heading angle.

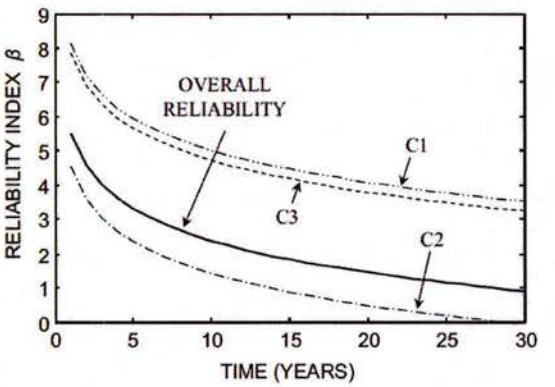

Figure 21 Time-variant fatigue reliability index for original individual operational states and the overall reliability index profile.

4.4. Conclusions

In this subsection, fatigue assessment of aluminum high-speed naval vessels with respect to individual operational conditions has been performed. In addition, an approach for the reliability-based fatigue assessment and life estimation has been proposed. Operational data of the ship, in terms of the time spent at each operational condition (i.e. sea state, heading angle, and speed), were used, in conjunction with the sea trial SHM data, to predict the long-term fatigue reliability of a ship detail. The hot spot structural stress approach was used for the fatigue assessment; however, the proposed methodology can be applied to any stress analysis method. The proposed approach allows to (a) evaluate the reliability-based fatigue life in a straightforward manner, (b) analyze the effect of different operational conditions on the fatigue damage accumulation to adjust the ship safe operational profile and minimize the probability of fatigue failures, (c) plan the ship route in order to minimize the fatigue damage accumulation, and (d) promote the real-world application of reliability-based methods using SHM information. The proposed fatigue life estimation method is applied to strain data of the HSV-2 obtained during the seakeeping trials of the vessel. The following conclusions can be drawn:

1- Some combinations of speeds, sea states, and wave headings have a significant effect on fatigue damage accumulation. These operational conditions should be identified and they should be avoided to prevent the accelerated damage to the ship structure.
2- The effect of the T-foil on the damage accumulation has to be investigated carefully for different operational conditions. For the analyzed vessel, it was found that at speeds of 30 and 15 knots, the damage accumulation is larger when the T-foil is deployed. However, for speed of 35 knots, the T-foil deployment significantly reduces the damage accumulation.
3- Although fatigue is a major limit state affecting the ship safety, other limit states, such as the serviceability and ultimate strength, should also be studied using SHM information including Bayesian updating.
4- The proposed approach enables the active integration of fatigue limit state in the life-cycle management maintenance optimization based on system reliability and life-cycle cost analysis can be performed, as well as the active route planning to minimize the fatigue damage accumulation at critical details during voyages

5. Risk-informed Optimal Routing of Ships Considering Different Damage Scenarios and Operational Conditions

The worldwide maritime transportation of goods and services rely on the proper ship routing. Decisions regarding the ship route are made according to the encountered sea conditions and ship strength capability, and are usually subjected to time constraint. The proper ship route planning relies on decision making tools that estimate the optimum ship direction and speed based on cost minimization and best estimated time of arrival (ETA). Sometimes, ships are forced to travel

along routes that put their structure at risk, potentially facing drastic drops of their operational safety. Therefore, it is crucial to include in the optimal routing the analysis of structural performance indicators such as reliability and risk, which account for the consequences of potential failures or malfunctions. It is also important to provide decision tools that prevent ship structures from down-crossing safety thresholds, which may cause important economic losses and loss of lives among the crew and/or passengers. Such an approach is developed in this investigation. The detailed approach, results, and discussion can be found in Decò and Frangopol (2013) and (2015).

The evaluation of the consequences due to potential failures or malfunctions plays a fundamental role in decision analysis. The use of reliability leads to decisions that do not account for any type of negative consequences. Therefore, every decision should actually be based on risk, which associates the probability of occurrence of specific events with the generated consequences, usually expressed as expected losses. The inclusion of risk, seen as a further performance indicator, can enhance structural safety analysis in order to provide the decision makers with a wide spectrum of options, also accounting for the economic aspect.

Among different types of hazards, such as fire, collision, grounding, the vulnerability of ship hulls is evaluated with respect to the flexural failure mode under normal as well as under extreme sea conditions and considering different ship operational conditions. Due to the fact that yielding or slight damage may be present within the structures of operating ships, different limit states *LSi* accounting for the occurrence of yielding and propagation of plastification throughout the hull are investigated. The following states *Si* are emphasized:

- State *S*1: the ship hull is within the elastic range and buckling has not occurred in the plates or in the stiffened panels.
- State *S*2: the ship hull is right over the elastic behavior, experiencing local buckling of the extreme stiffeners with respect to the neutral axis, which induces local plastification. In order to allow small regions of the hull extremities to plastify, it is assumed that the plasticized area is located within the extreme plates and up to 20% of the largest distance to the neutral axis. Buckling of the compressed extreme stiffeners occurs.
- State *S*3: the plastification propagates throughout the section reaching values between 20% and 50% of the largest distance to the neutral axis. Buckling effects are extended through a large portion of the stiffened panels. The hull deforms significantly and ship service is at risk.
- State *S*4: the plastification propagates throughout the section (greater than 50% of the largest distance to the neutral axis) until the ultimate flexural capacity is reached. Ship serviceability is compromised and the collapse is imminent due to large deformations.
- State *S*5: ship collapse occurs.

The above mentioned five states (*S*1 to *S*5) are evaluated by investigating four different limit states: yielding (*LS*1), plastification propagation up to 20% (*LS*2) and 50% (*LS*3) of the largest distance to the neutral axis, respectively, and ultimate capacity (*LS*4). The reaching of a specific limit state is in general due to the combined effects of vertical and horizontal bending moments. Therefore, based on the studies of Paik *et al.* (1996) and Gordo and Guedes Soares (1996, 1997),

for each limit state the associated hull strength is given by the following equation providing limit state contours:

$$\left(\frac{M_v}{M_{v,LSi}}\right)^{c_{1,LSi}} + \left(\frac{M_h}{M_{h,LSi}}\right)^{c_{2,LSi}} = \delta \tag{38}$$

where δ is a parameter, M_v and M_h are the vertical and horizontal bending moments, respectively, due to sea load effects, $M_{v,LSi}$ and $M_{h,LSi}$ are the vertical and horizontal flexural capacities associated with a specific limit state LSi, respectively, and $c_{1,LSi}$ and $c_{2,LSi}$ are parameters. M_v and $M_{v,LSi}$ can be taken as either sagging or hogging, depending on the load combination under analysis.

Time processes may decrease the mechanical properties of the hull, and corrosion effects may generate loss of thickness throughout the hull section. This causes the deterioration of the section modulus, thus reducing the section flexural capacity. Therefore, considering the effects of corrosion on ship structures, Eq. (38) can be rewritten as:

$$\left(\frac{M_v}{M_{v,LSi}(t)}\right)^{c_{1,LSi}} + \left(\frac{M_h}{M_{h,LSi}(t)}\right)^{c_{2,LSi}} = \delta \tag{39}$$

where t is time.

5.1. Reliability Analysis

Other than considering different ship operational conditions, reliability analysis is also conducted with respect to different limit states LSi previously introduced. Ship reliability analysis can be performed based upon the knowledge of the probability distributions of the flexural strengths and the statistical descriptors of the load effects, later discussed. Based on Eq. (39), the time-dependent failure probabilities and the corresponding reliability indices are based on the time-dependent performance function $G_{LSi,SE,U,H}(t)$, associated with a LSi and for different operational conditions. This function is:

$$G_{LSi,Hs,U,H}(t) = \delta - \overbrace{\left(\frac{x_{sw}M_{sw} + x_w k_W \left(M_{wv,Hs,U,H} + k_D M_{WH}\right)}{x_R M_{v,LSi}(t)}\right)^{c_{1,LSi}}}^{VBM} - \overbrace{\left(\frac{x_w M_{wh,Hs,U,H}}{x_R M_{h,LSi}(t)}\right)^{c_{2,LSi}}}^{HBM} \tag{40}$$

where the subscripts Hs, U, and H refer to significant wave height, ship speed, and ship heading angle, respectively, δ is a parameter theoretically set to one, x_R, x_{sw}, and x_w are parameters accounting for the model uncertainties associated with the resistance determination, still water bending moment prediction, and wave-induced bending moment prediction, respectively, k_W is the correlation factor for the wave-induced bending moment set to one, k_D is the correlation factor between wave-induced and dynamic bending moments, M_{sw} is the still water bending

moment, $M_{wv,Hs,U,H}$ and $M_{wh,Hs,U,H}$ are the vertical and horizontal wave-induced bending moments given by linear theory, respectively, M_{WH} is the whipping bending moment, $M_{v,LSi}$ and $M_{h,LSi}$ are the vertical and horizontal flexural capacities, and $c_{1,LSi}$ and $c_{2,LSi}$ are parameters referring to the selected *LSi*. Depending on the load effects under analysis, the terms M_{sw}, $M_{wv,Hs,U,H}$, $M_{v,LSi}$, $c_{1,LSi}$, and $c_{2,LSi}$ assume different values for sagging and hogging.

The evaluation of the probability of failure associated with the ultimate capacity (*LS*4) and the probabilities of exceedance of three different limit states (*LS*1, *LS*2, and *LS*3) are necessary in order to relate the right level of consequences. These time-dependent probabilities $P_{LSi,Hs,U,H}(t)$ are generally calculated as follows:

$$P_{LSi,Hs,U,H}(t) = P\left[G_{LSi,Hs,U,H}(t,\mathbf{X}) < 0\right] = \int_{G_{LSi,Hs,U,H}(t,\mathbf{X})<0} f(t,\mathbf{X})dx \tag{41}$$

where $f(t,\mathbf{X})$ is the joint PDF of the considered random variables $\mathbf{X} = x_1, x_2,\ldots,x_k$ at a given time t. Given that usually this integral cannot be solved analytically, these probabilities can be evaluated using approximate methods such as the first-order reliability method (FORM), among others. The relationship between the time-dependent reliability index $\beta_{LSi,Se,U,H}(t)$ and probability $P_{LSi,Hs,U,H}(t)$ for a given *LSi* and for different ship operational conditions is:

$$\beta_{LSi,Hs,U,H}(t) = \Phi^{-1}\left(1 - P_{LSi,Hs,U,H}(t)\right) \tag{42}$$

where Φ^{-1} is the inverse standard normal distribution function.

In order to find the time-dependent probabilities $P_{Si,Hs,U,H}(t)$ of the hull being in the previously defined states *S*1 to *S*5, which are based on the exceedance probabilities $P_{LSi,Hs,U,H}(t)$ for the limit states *LS*1 to *LS4*, a procedure similar to the fragility analysis, is used herein. The difference is that variables such as sea elevation and ship speed and heading angle are those that affect the loads on the hull. Since the five introduced states consider progressive plastification of the hull (*S*1 to *S*5), the probabilities of the hull being in specific states are:

$$\begin{cases} P_{S1,Hs,U,H}(t) = 1 - P_{LS1,Hs,U,H}(t) & i = 1 \quad \text{before yielding} \\ P_{Si,Hs,U,H}(t) = P_{LS(i-1),Hs,U,H}(t) - P_{LSi,Hs,U,H}(t) & 2 \le i \le 4 \quad \text{yielding propagation} \\ P_{S5,Hs,U,H}(t) = P_{LS4,Hs,U,H}(t) & i = 5 \quad \text{failure} \end{cases} \tag{43}$$

5.2. *Consequences Analysis*

This section presents the consequence analysis including specific costs associated with the potential failure of a ship hull or the exceedance of specific limit states such as those associated with the propagation of plastification. Direct consequences are the losses due to the damage or the failure itself, whereas indirect consequences are those related to system failure or malfunctions that induce external monetary losses. The main indirect losses/costs for marine structures can be summarized as those due to (IMO 1997, Ayyub *et al.* 2002,): injuries and

fatalities to passengers and crew, damage to ship equipment, transported goods, and port facilities, and commercial and environmental impacts, among others.

The focus of this study is risk-informed routing of ships based on the quantification of the hull structural safety (i.e. in terms of risk); therefore direct consequences, including construction and rehabilitation costs, are emphasized among other types of potential consequences and operational costs. This paper provides a direct link between the structural performance in terms of hull flexural strength and the economic direct impact, however indirect consequences can be accommodated in the proposed framework. Consequence analysis uses an economic approach and a monetary value expressed in United States Dollar (USD). The considered direct costs are:

- *Construction costs* C_{Con}: weight-based costs of construction. These costs are evaluated by using the equations proposed by Miroyannis (2006) based on empirical Cost Estimation Relationships (CERs). This method is in agreement with the NAVY standards, being the NAVY's cost estimates mostly based on weights only. Accordingly, considering the Ship Work Breakdown System (SWBS), ship costs are subdivided in categories, such as structure, propulsion, and electrical, among others. In this paper, the estimated costs (USD) are obtained considering ship preliminary design and the structural SWBS category denominated "100". These costs are given by (Miroyannis 2006):

$$C_{Con} = \overbrace{CF \times 177 \times WGT_{100}^{\ 0.862}}^{\text{Labor Manhours}} + \overbrace{800 \times WGT_{100}}^{\text{Material Dollars}} \tag{44}$$

where

$$CF = STF \times SF \tag{45}$$

$$SF = 32.47 \times DISPL^{-0.3792} \tag{46}$$

in which CF is the complexity factor, WGT_{100} is the weight of the SWBS 100 (long tons), STF is the ship type factor, SF is the size factor, and $DISPL$ is the ship full load displacement (long tons).

- *Rehabilitation costs* $C_{Reh,Si}$: considered as fractions of the ship construction costs based on the estimated level of damage. These costs are evaluated as:

$$C_{Reh,Si} = d_{r,Si} C_{Con} \tag{47}$$

where $d_{r,Si}$ is the damage ratio (i.e. the proportionality factor between ship repair costs and the ship construction costs). The criterion adopted for the quantification of the damage is based on the percentage of plasticized area within the considered hull section. Therefore, the damage ratios associated with each specific state Si are evaluated in accordance with each of the specified hull states. Accordingly, state $S1$ does not generate any consequences, since by definition the hull section is within the elastic range and buckling has not occurred, whereas the other states cause direct consequences proportional to the damaged area. In the cases of the ship being in states $S2$ to $S4$, C_{Con} is assumed to refer to the portion of the hull surrounding

the damaged midship section damage, while for the state *S*5, C_{Con} is assumed to account for the structure of the entire ship hull.

5.3. *Risk Assessment*

Risk is defined as the combination of occurrences and consequences of events generated by specific hazards. The risk $R(t)$ referred to a specific time t can be expressed as

$$R(t) = \int\int ... \int \delta(t, \mathbf{X}) f(t, \mathbf{X}) dx \tag{48}$$

where $\delta(t,\mathbf{X})$ represents the consequences and $f(t,\mathbf{X})$ is the joint PDF of the considered random variables $\mathbf{X} = x_1, x_2, \ldots, x_k$. The solution of Eq. (48) is not obvious; therefore, risk is evaluated by considering an approach that accounts for the discrete states associated with the different hull damages described previously. Since the five states are mutually exclusive and collectively exhaustive, time dependent total risk $R_{Hs,H}(t)$ for a given set of *Hs*, *U*, and *H* can be obtained as:

$$R_{Hs,U,H}(t) = \sum_{s=S1}^{S5} C_{Si} P_{Si,Hs,U,H}(t) \tag{49}$$

where C_{Si} are the total consequences associated with specific states *Si*. The time-dependent direct risk $R_{D,Hs,H}(t)$ can be obtained as:

$$R_{D,Hs,U,H}(t) = \left[\sum_{s=S2}^{S4} C_{Reh,Si} P_{Si,Hs,U,H}(t) \right] + C_{Con} P_{S5,Hs,U,H}(t) \tag{50}$$

5.4. Probabilistic *Hull Strength*

FEM-modeling is used to obtain vertical and horizontal moment-curvature relationships in order to investigate structural performance, and provide indications about ship reliability, as later discussed in the case study. In order to achieve this goal, a detailed non-linear response analysis of the hull, accounting for both geometric and material non-linearity, is performed.

While the use of conventional non-linear FEM is possible for deterministic analysis, this technique is computationally demanding, especially for stochastic analyses of the ship's strength, involving a potentially high number of simulations (e.g. for reliability analysis). Therefore, in order to account for uncertainties and significantly reduce the computational costs to an acceptable level, FEM is used in combination with the Response Surface Method (RSM) (Bucher and Bourgund 1990). The RSM consists in the execution of deterministic FEM-analyses at specific values of the considered random variables. The obtained results, representing the responses, are collected and summarized into a RSM-equation originated by regression analysis. For instance, if a second-order interpolating polynomial is selected, the fitting RSM-equation leads to:

$$R = \alpha_0 + \sum_{i=1}^{k} \alpha_i x_i + \sum_{i<j}^{k} \alpha_{ij} x_i x_j + \sum_{i=1}^{k} \alpha_{ii} x_i^2 \tag{51}$$

where R is the response, α_0, α_i, α_{ij}, and α_{ii} are the polynomial coefficients to be determined, i and j are indices referring to the selected random variables x_i and x_j, respectively, and k is the total number of random variables. Once all the responses are collected from the FEM-simulations, the coefficients α in Eq. (51) can be estimated by the method of the least squares

5.5. Risk informed route optimization

In order to fully exploit the introduced framework to assess risk due to expected losses, among other potential applications, the risk-informed route optimization based on mission-oriented reliability (i.e. accounting for short period load effects) is introduced in this section. Once risk has been evaluated for a given set of operational conditions, the optimal route of a ship under various weather conditions can be obtained. Assuming that a weather forecast is given for a specific sea region (described by an x-y Cartesian coordinate system) and that a ship has to travel between the points O (origin) and D (destination) within this region, the above mentioned optimization problem can be solved by discretizing the travel in N segments, that are described by initial and end points in the x and y coordinates. For each initial point of each N-th segment, a ship speed U has to be provided. Assuming that the x-axis is discretized in a fixed number N of intervals, the optimal route is determined by the evaluation of the N-1 y coordinates required to describe the N route segments. Accordingly, the optimization problem can be formally addressed as follows:

Given: sea weather map that includes sea elevation in terms of significant wave height, wave direction, and risk with respect to different operational conditions at a specific ship age t

find: a set of ship speeds U_i and coordinates y_i

$$U_i \qquad \forall i = 1, 2, ..., N \tag{52}$$

$$y_i \qquad \forall i = 1, 2, ..., N-1 \tag{53}$$

to minimize: the estimated time of arrival ETA and the risk R

$$\min\{ETA, R\} \tag{54}$$

subjected to the constraints:

$$U_{\min} \le U_i \le U_{\max} \qquad \forall i = 1, 2, ..., N \tag{55}$$

$$y_{\min} \le y_i \le y_{\max} \qquad \forall i = 1, 2, ..., N-1 \tag{56}$$

where N is the number of the travel discretization based on the map dimensions with respect to the x-axis, U_{min} and U_{max} are the minimum and maximum allowable ship speed, respectively, and y_{min} and y_{max} are the bounds of the map in the y-axis direction. A potential sea weather map, describing the routing optimization is reported in the figures describing the optimization process of the case study later introduced. Although further parameters and constraints may be relevant for the selection of the optimal routes, the used approach shows that decisions can be based on

risk. The inclusion of further constraints can be accommodated in the proposed framework, making the decision process even more accurate. Since this optimization problem is not described by a closed form solution, the use of a heuristic optimization tool such as the GA is preferable with respect to classical gradient-based methods. Therefore, in this paper, the optimization process is carried out by multiobjective GA provided by the software MATLAB, which uses a modified version of the NSGA-II algorithm. The Pareto-optimal set represents the optimal routes guaranteeing that the obtained solutions lead to an optimal result for both objective functions. Therefore, any point belonging to this set can be chosen by the decision makers depending on the acceptable level of risk and on the allowable time to complete the travel. Another important aspect, addressed in the case study, is to investigate the optimal routing of aged ships, i.e. accounting for the loss of strength of the hull due to corrosion effects. This analysis can be performed by repeating the same optimization problem in order to show how decisions may vary when a ship with greater structural vulnerability is considered.

5.6. Results and Discussion

The proposed framework is applied to the Joint High-Speed Sealift (JHSS) discussed in Devine (2009) having the following properties: length between the perpendiculars LBP = 290 m, breadth b = 32 m, height h = 22.3 m, block coefficient Cb = 0.4835, and full load displacement DISPL = 34,779.1 Mtons. Figure 22(a) shows the drawing developed with the software FREE!ship (2006).

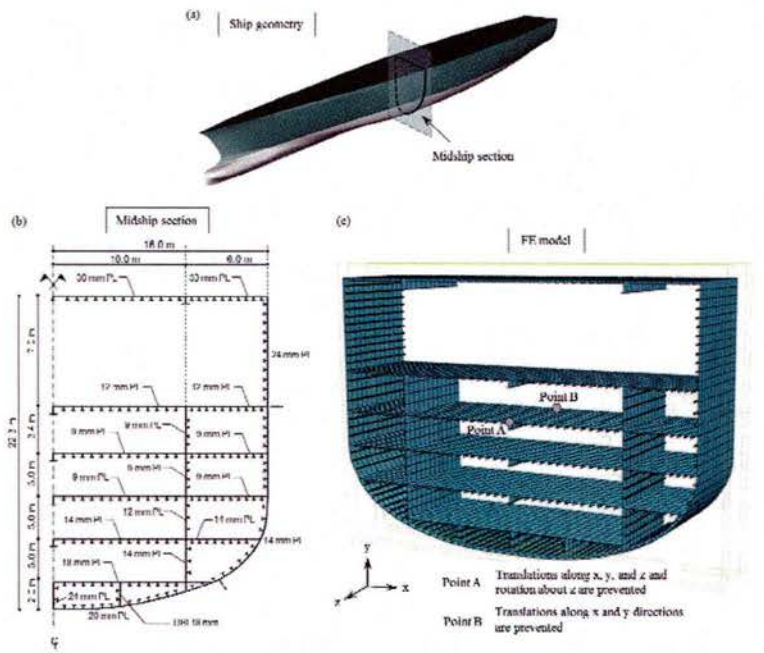

Figure 22. (a) Model of the analyzed JHSS built by the software FREE!ship (2006), (b) geometry of the midship section (145 m aft FP), and (c) FEM-model of the part of the hull that includes the midship section built with ABAQUS

A total of 18,216 shell elements and 19,528 nodes are generated for the model. Both material and geometric non-linearities are considered. Figure 23 shows the printouts of the results obtained with ABAQUS in terms of Von Mises mean stress contours in the case of hogging curvature. The images show the midship section stresses for limit states LS1 (Fig. 23(a)), LS2 (Fig. 23(b)), LS3 (Fig. 23(c)), and LS4 (Fig. 23(d)).

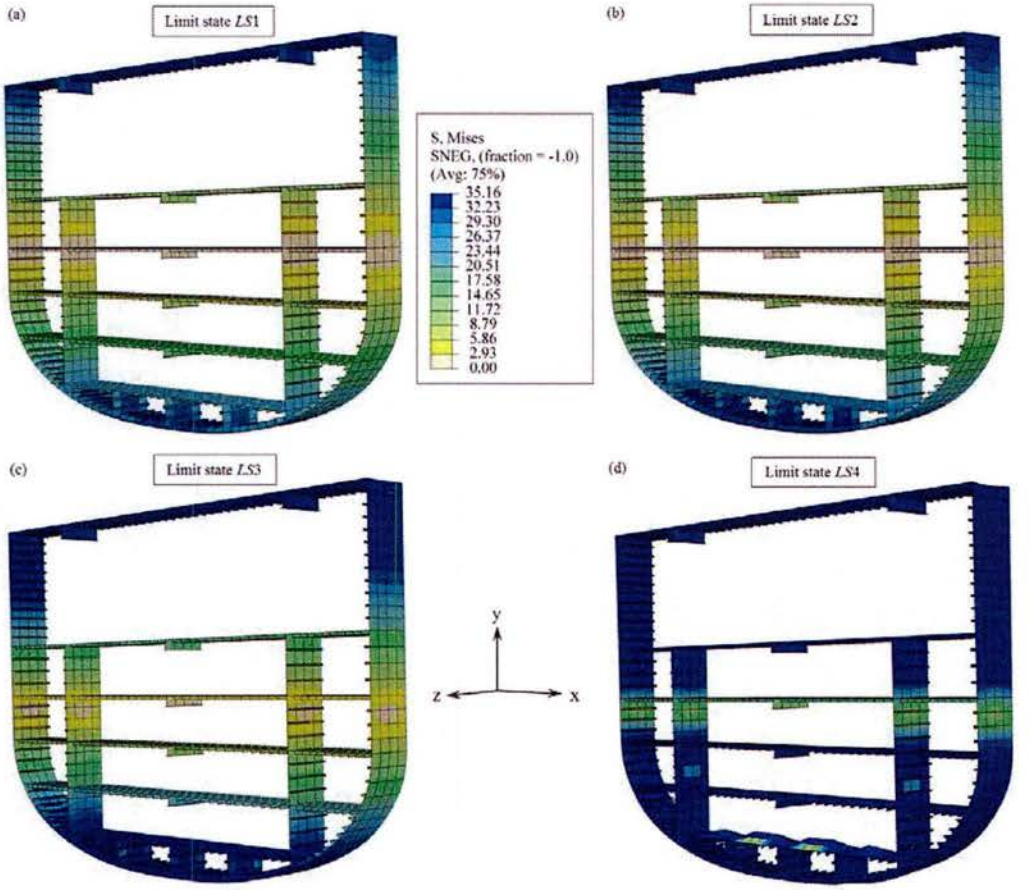

Figure 23. Von Mises mean stress contours of the hull midship section for the four considered limit states LSi.

In order to perform risk assessment, the probabilities associated with reaching the defined four limit states (*LS*1 to *LS*4) are evaluated. The software RELSYS is used to perform reliability analysis. Using polar representation, Figure 24(a) shows the reliability indices associated with the four limit states for intact ship (t = 0 years) and for aged ship (t = 30 years), which are represented at the right and left sides, respectively, for sea state 5 (Hs = 2.74 m) and ship speed of 10 m/s. Obviously, the reliability associated with the first yielding (*LS*1) is lower than the reliability with respect to the ship ultimate capacity (*LS*4) for all the considered operational conditions. Fig. 24(b) reports on the reliability associated with *LS*4 for intact (right side, t = 0) and aged (left side, t = 0) ship at a fixed speed of 10 m/s and for sea states 4, 5, and 6. Since it is

found that the effects induced by hogging are more severe than those induced by sagging, only hogging is considered. The Cartesian plots associated with the polar representations of Fig. 24(a) and 24(b) are shown in Fig. 24(c) and 24(d), respectively.

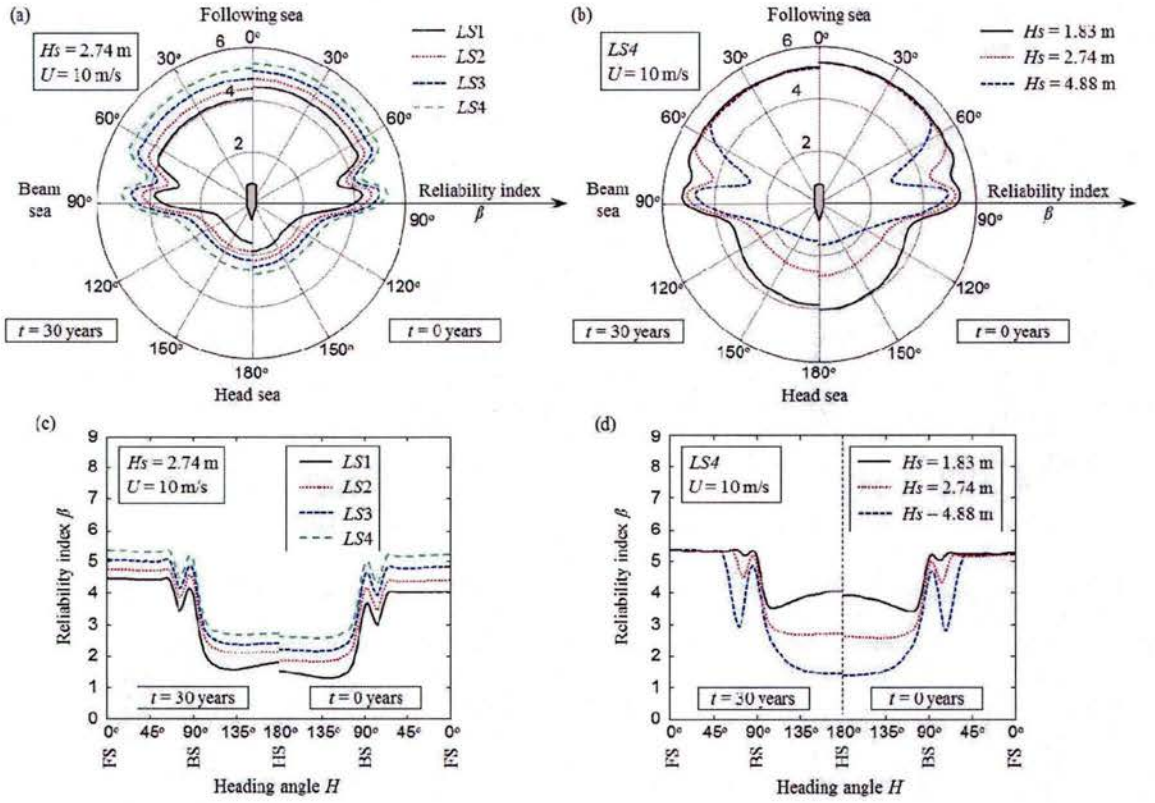

Figure 24. Polar profiles of the reliability indices for intact (right side, t=0 years) and aged (left side, t=30 years) ship with respect to (a) four limit states given Hs=2.74 m and ship speed of 10 m/s, and (b) ultimate capacity (LS4) for ship speed of 10 m/s by varying significant wave height. Associated Cartesian plots of the reliability indices for intact and aged ship with respect to (c) four limit states and (d) ultimate capacity varying significant wave height.

Finally, risk is assessed for each state *Si* and for all the considered operational conditions. Figure 25(a) shows the direct risk profiles given ship speed of 10 m/s and *Hs* = 2.74 m. It can be noticed that the obtained risk profiles cross each other depending on both the probabilities P_{Si} and the evaluated magnitude of direct costs. Direct risk for *S*1 is null, given that the relevant damage ratio is assumed equal to 0 and, therefore it is not reported in Fig. 25(a). The profile of the total direct risk is shown in Fig. 25(b).

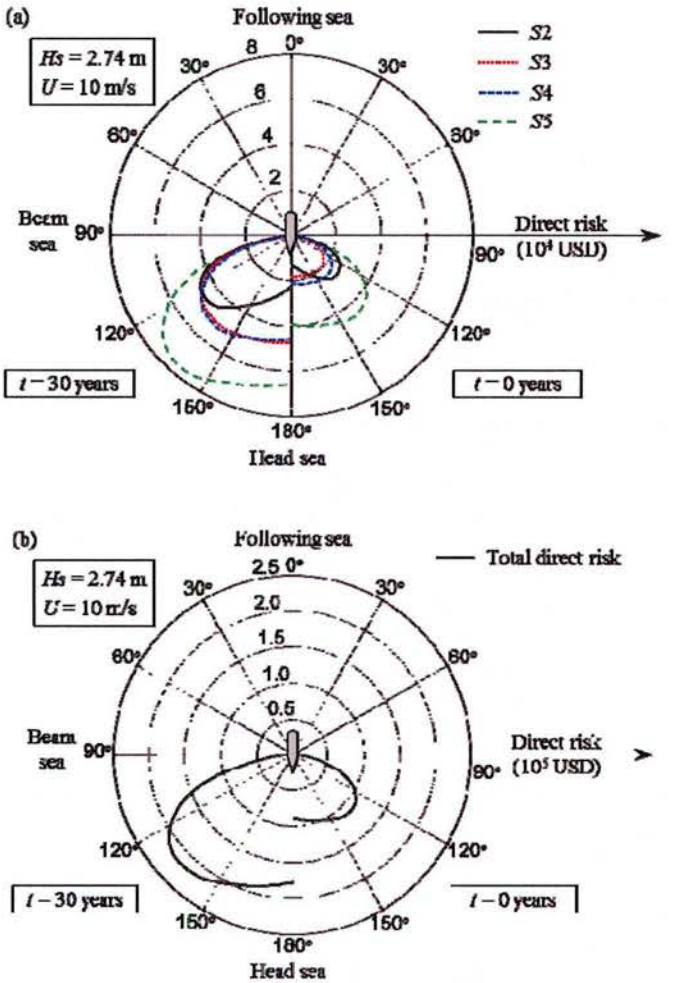

Figure 25 Polar profiles of the direct risk for intact (right side, t=0 years) and aged (left side, t=30 years) ship with respect to (a) four states given Hs=2.74 m and ship speed of 10 m/s and (b) ultimate capacity (LS4) for ship speed of 10 m/s.

In order to provide an application on risk-informed optimal routing of ships, assumptions have to be made, such as the origin and destination of the route, and the sea weather map for the studied area. Figure 26 shows the assumed sea weather map, including a qualitative path, where the *x*- and *y*-axis ranges are assumed to be 1000 km, and O ≡ (1000 km, 200 km) and D ≡ (0 km, 400 km) indicate the points of origin and destination, respectively. In the map, the shadings show the intensity of the sea expressed in terms of significant wave height, and ranging from 1.07 and 6.10, equivalent to lower sea state 3 and upper sea state 6, respectively, and the arrows report on the direction of propagation of the waves, given the weather system. Two areas of disturbance represented by two potential storms are included in the graphical representation. According to the optimization problem previously formulated, the *x*-axis has been divided in 15 segments (N = 15), representing the discretization of a potential journey. Based on this discretization, optimal sets composed by 15 ship speeds U_i and 14 coordinates y_i are evaluated. These design variables

are subjected to the constraints, assuming that the relevant ranges are 4 m/s $\leq U_i \leq$ 20 m/s and 0 km $\leq y_i \leq$ 1000 km.

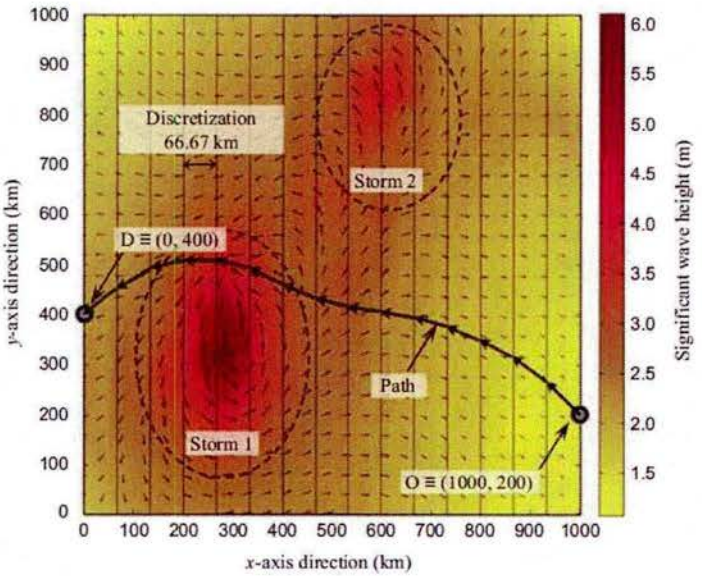

Figure 26 Assumed discretized sea weather map of the considered squared area with edges of 1000 km, in which the shadings report on the significant wave height and the thin arrows show the direction of propagation of the waves. The thick arrows represent a potential path connecting the origin point O and the destination point D.

Figure 27 shows the Pareto-optimal set for the case of intact ship (t = 0 years). The two objectives are the estimated time of arrival *ETA* (h) and the normalized direct risk R_D (USD/km) over the length of the shortest followed path. These are conflicting objectives, because depending on the given weather map, the fastest and shortest solution (point A of the Pareto front) is associated with a high level of risk. Decision makers can adjust path and speed depending on the allowable risk. Three Pareto solutions are selected among the others and are denominated A, B, and C. (Fig. 27). Figure 28(a) shows the paths associated with the three selected solutions. It is noticed that all the three paths share some common segments, especially while traveling in the central part of the journey. These solutions are associated with the values of the objectives as provided in Fig. (27). Path C covers the longest distance, avoiding the represented storm 1 heading south, whereas path B heads north. The shortest path A directly crosses the storm. Figures 28(b, c, and d) show the ship speed, the reliability index associated with ultimate failure, and the normalized direct risk, respectively, for each of the 15 segments dividing the map. The paths A and B are covered at the maximum speed of 20 m/s along the entire trip, leading to an important reduction of ETA to the detriment of mission reliability (Fig. 28(c)), which reduces significantly whenever severe sea state is encountered. The ETA of path C is larger due to the overall reduced traveling speed (Fig. 28(b)) and to the longer traveled distance. Although only three solutions are shown for sake of clarity, other Pareto solutions are available to decision makers.

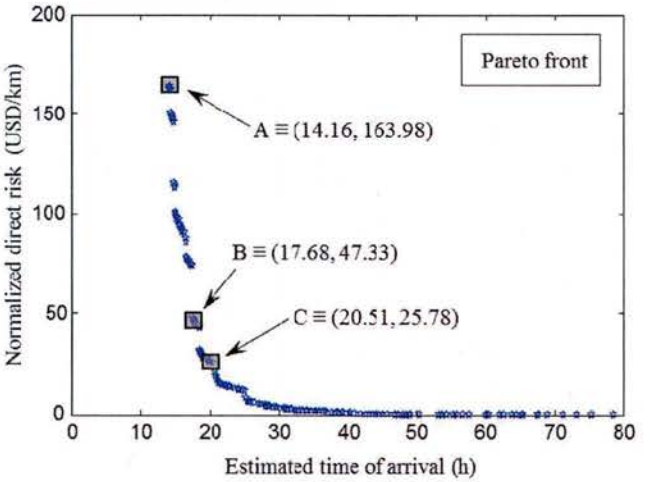

Figure 27 Pareto front of the optimization problem obtained by minimizing both estimated time of arrival and normalized direct risk. Three representative solutions denominated A–C are selected in order to evaluate the relevant mission parameters.

5.7. Conclusions

This investigation uses risk as a performance indicator accounting for the consequences induced by different limit states, with the purpose of evaluating the optimal routing of ships. Direct risk assessment of ships can be performed with respect to discrete hull damage states and for a large spectrum of operational conditions. Mission parameters such as ship speed and heading angle, structural safety, ETA, and traveled distance are properly assessed for the case of the Joint High-Speed Sealift, hypothetically traveling between two points for an assumed sea weather map. Optimization has been conducted for both the case in which the ship is intact and when the effects due to corrosion induce deterioration of the structural performance leading to higher direct risk.

The following conclusions are obtained:

1. Direct risk of ships can be assessed considering different ship limit states and with respect to several operational conditions. It is found that direct risk profiles associated with specific states can cross each other depending on the magnitudes of the probabilities of the hull being in specific states and direct costs. Overall, greater direct risk is associated with head sea.
2. The inclusion of negative consequences in decision analysis is of paramount importance. Different travel paths can be followed by ships, thus minimizing the effects of such consequences. A future challenge is represented by the development of rules and specifications that address this aspect in order to adequately warn decision makers on ship reliability.
3. The results obtained from the optimization show that several solutions can be adopted depending on the acceptable risk and on the allowable ETA. All the solutions, except for the shortest and fastest one, provide directions that avoid the assumed storm in order to reduce direct risk.

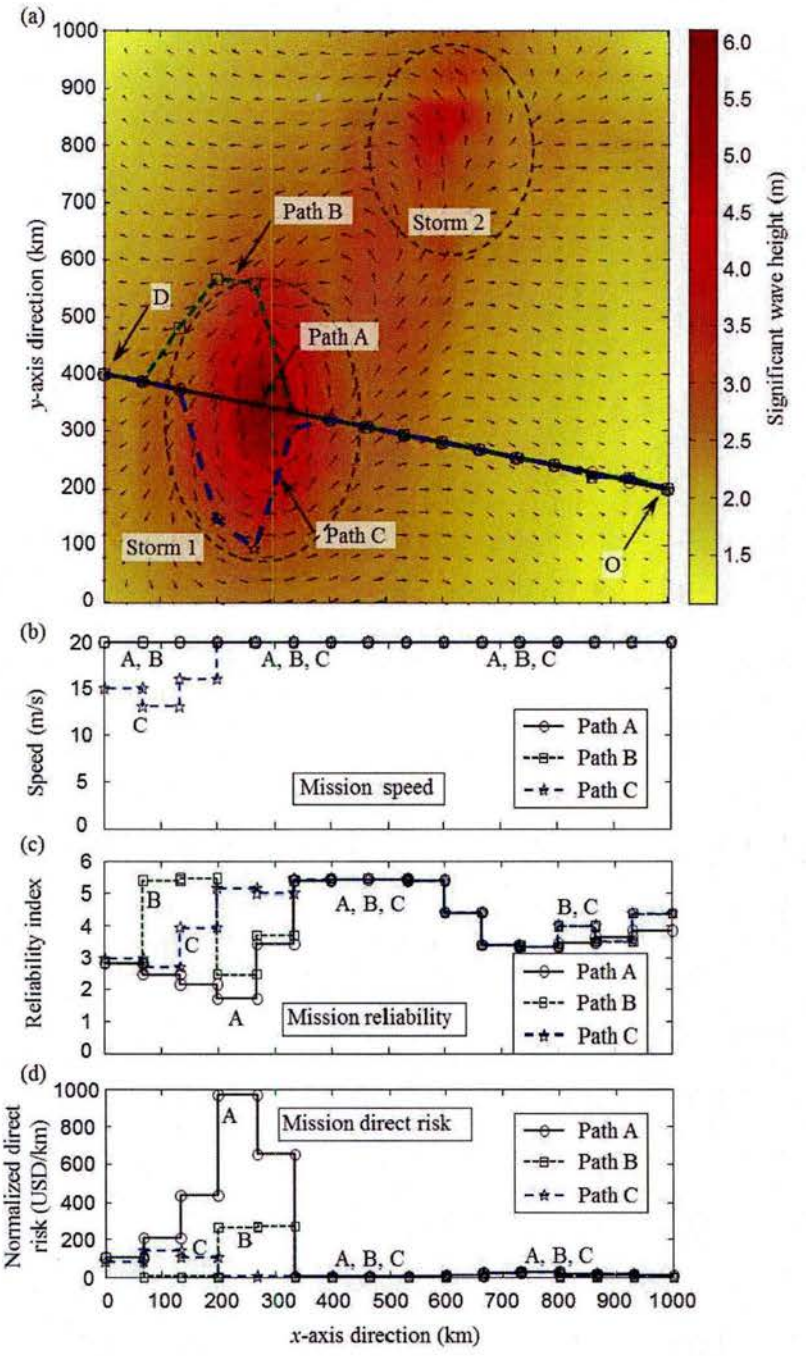

Figure 28 (a) Paths of the three selected solutions A–C represented in the assumed sea weather map. Profiles of (b) ship speed, (c) mission reliability index associated with ultimate failure and (d) normalized direct risk for each of the three solutions.

Although it is known that other factors, such as traveling comfort and fuel consumption may play a role within this optimization problem, the importance of risk-informed decision making is highlighted in this paper. The inclusion of other factors may be a future development of the proposed approach discussed herein.

6. Real-time Risk of Ship Structures Integrating Structural Health Monitoring Data: Application to Multi-objective Optimal Ship Routing

This investigation develops a risk-informed approach for ship structures that integrates structural health monitoring (SHM) information. As an application, an approach on real-time optimal short range routing of ships is also developed. A novel closed-form solution for short term statistics based on Rayleigh prior distribution and a simulation-based technique are proposed for Bayesian updating. Finally, optimal short range routing of ships is accomplished by solving three-objective optimization problem, accounting for the minimization of estimated time of arrival, mean total risk, and fuel cost, given sea weather maps and origin and destination points. Weather forecast, associated with different time frames, is also included within the developed framework. The detailed approach, results, and discussion can be found in Decò and Frangopol (2015).

6.1. Structural Health Monitoring

The first aspect to be considered in order to make near real-time decision is the availability of further data, additional to those used for the initial assessment, which allows the decision to be more accurate within tight time steps. The principal quantity of interest to be updated is represented by the VBM induced by waves $M_{wv,Hs,U,H}$, which in this paper is treated as a random variable.

The SHM data used in this paper were obtained by Dr. Devine and his co-workers during different testing sessions of a Froude-scaled test model of a NAVY's Joint High-Speed Sealift (JHSS) at the Naval Surface Warfare Center, Carderock Division - Maneuvering and Sea Keeping (NSWCCD - MSK) basin, and provided us (Devine 2009). Thus, the collected SHM data in terms of VBM are scaled up by using the proper Froude-scaling factor in order to account for the load effects associated with the full-scale ship. The recorded raw signal, obtained by merging different test runs includes the effects of both low- and high-frequency responses, that are associated with the most regular part of the wave excitation and the effects of hull vibrations in terms of slam-induced hull whipping, respectively (Devine 2009). Depending on the availability of SHM data for different ship operational conditions, in this paper reliability analysis will include those available runs associated with a specific combination of *Hs*, *U*, and *H*, therefore the updated limit state equation is

$$G'_{LSi,Hs,U,H}(t) = \delta - \left(\frac{x_w M_{wh,Hs,U,H}}{x_R M_{h,LSi}(t)} \right)^{c_{2,LSi}} - \left(\frac{x_{sw} M_{sw} + x_w k_W \left(\overbrace{M_{low,Hs,U,H}}^{\text{Updated}} + k_D \overbrace{M_{high,Hs,U,H}}^{\text{Directly from SHM}} \right)}{x_R M_{v,LSi}(t)} \right)^{c_{1,LSi}} = 0 \tag{57}$$

where $M_{low,Hs,U,H}$ and $M_{high,Hs,U,H}$ are the updated low-frequency and the obtained high-frequency VBM, respectively. Similarly, also the HBM can be updated based upon the availability of SHM data.

In order to separately investigate the effects of low- and high-frequency VBM, the raw signal needs to be filtered and analyzed independently. Butterworth filter is used for this purpose. The cutoff frequency, which subdivides the frequency-domain into two parts containing the two frequency peaks, is properly chosen by analyzing the raw signal within the frequency-domain obtained with the Fourier transform of the raw signal. Additionally, the noise associated with very high frequency is removed from the raw signal.

The filtered signal oscillates from negative to positive values, representing sagging and hogging VBM, respectively (Devine 2009). At this stage, the signal must be mathematically characterized by developing a mathematical estimation of the data (i.e. PDF), and by assessing the relevant statistical descriptors. In order to do so, the peaks of the signal are extracted, and their values are stored. An algorithm has been used for this purpose, implemented with the software MATLAB. It is found that the best fit for the filtered low-frequency VBM is provided by using the Rayleigh distribution. This is in accordance with the theory behind short term statistics prediction. Whereas, for high frequency peaks, exponential distribution is selected because it provides better goodness-of-fit compared to other distributions. Therefore, these high-frequency peaks are distributed as follows

$$f\left(M_{high,Hs,U,H}\right) = \frac{e^{\frac{-M_{high,Hs,U,H}}{\lambda_{Hs,U,H}}}}{\lambda_{Hs,U,H}} \qquad \lambda_{Hs,U,H}, M_{high,Hs,U,H} \geq 0 \tag{58}$$

where $\lambda_{Hs,U,H}$ is the mean of a specific monitored combination of *Hs*, *U*, and *H*.

6.2. Bayesian Updating

The performance assessment based only on the SHM data, and disregarding the original information, can be restrictive, and may provide bias results. In this context, the Bayesian approach makes it possible to use the additional monitoring information in conjunction with the already available initial information. Briefly, the Bayesian approach mainly deals with the parameters θ_j, which are described by their associated PDF called "prior PDF" $f'(\theta)$. In turns, the

prior PDF has parameters itself, that are often called "hyperparameters" in order to distinguish them from the basic parameters of the underlying random variable X (e.g. VBM). Besides, discrete values are collected from SHM. Assuming that x_1, x_2,...x_j,..., x_n are the stored observations (i.e. the values of the extracted peaks of the VBM), then the likelihood function $L(\theta)$ assuming a given parameter θ is

$$L(\theta) = \prod_{j=1}^{n} f_X(x_j \mid \theta) \tag{59}$$

where $f_X(x_j|\theta)$ is the PDF of the random variable X evaluated with the SHM data value x_j, given the PDF parameter θ. Based on the Bayes' theorem, the posterior PDF $f''(\theta)$, i.e. the updated PDF of the parameters θ_j, is obtained by combining the prior PDF with the likelihood of the available observations as follows

$$f''(\theta) = kL(\theta)f'(\theta) \tag{60}$$

where k is the normalizing constant given as follows

$$k = \frac{1}{\int_{-\infty}^{\infty} L(\theta)f'(\theta)d\theta} \tag{61}$$

The expected value of parameter θ is commonly used as Bayesian estimator; therefore, by using the method of moments, the updated parameter θ is given by

$$\hat{\theta}'' = \int_{-\infty}^{\infty} \theta f''(\theta)d\theta \tag{62}$$

The implementation of SHM observation through Eq. (59) and the closed-form solution for Eq. (61) are not always achievable. Therefore, numerical based techniques, such as Markov chain Monte Carlo, Metropolis-Hastings algorithm, and slice sampling algorithm, among others, may be used. Both closed-form solution and simulation-based method are used herein.

In this study a novel analytical solution for the updating problem of structural performance, based on the collection of structural responses induced by wave effects, is developed. It is always easier to provide closed-form solution to the Bayes' problem when prior and posterior distributions are conjugated, i.e. belong to the same family. In this analysis, short term statistics has been used, thus the distribution of the prior information follows the Rayleigh distribution with mode α given by

$$\alpha = \sqrt{m_{0,Hs,U,H}} \tag{63}$$

Since the wave peaks follow the Rayleigh distribution, it is reasonable to assume that the mode α is a random variable itself, following the Rayleigh distribution. This new distribution represents the prior distribution $f'(\theta)$ of the parameter θ, defined as follows

$$f'(\theta) = \frac{\theta}{\alpha^2} e^{-\frac{\theta^2}{2\alpha^2}} \qquad \alpha, \theta \geq 0 \tag{64}$$

It can be noticed that the mode α is the hyperparameter of the prior distribution $f'(\theta)$. Recalling that the wave peaks follow the Rayleigh distribution, the likelihood function of the observations $x_1, x_2, \ldots x_j, \ldots, x_n$ given the parameter θ is

$$L(\theta) = \frac{e^{-\frac{1}{2\theta^2}\sum_{j=1}^{n} x_j^2} \prod_{j=1}^{n} x_j}{\theta^{2n}} \qquad \theta \geq 0 \tag{65}$$

Hence, the posterior distribution $f''(\theta)$ of the parameter θ, is given by

$$f''(\theta) = \frac{k e^{\frac{\theta^2}{2\alpha^2} - \frac{1}{2\theta^2}\sum_{j=1}^{n} x_j^2} \prod_{j=1}^{n} x_j}{\alpha^2 \theta^{2n-1}} \qquad \theta \geq 0 \tag{66}$$

where the normalizing constant k is obtained by solving Eq. (61), but integrated within the interval $[0, +\infty]$, because both $f'(\theta)$ and $L(\theta)$ are defined for $\theta \in [0, +\infty]$. Thus, k, handled with the software Mathematica, becomes

$$k = \frac{\alpha^{n+1} \left(\sum_{j=1}^{n} x_j^2 \right)^{\frac{n-1}{2}}}{\text{besselk}\left[n-1, \sqrt{\frac{1}{\alpha^2} \sum_{j=1}^{n} x_j^2} \right] \prod_{j=1}^{n} x_j} \tag{67}$$

where besselk[•] is the modified Bessel function of the second kind. After some math passages, developed with Mathematica and not reported here, the expected value of parameter θ is provided as follows

$$\hat{\theta}'' = k e^{-\sqrt{\frac{1}{\alpha^2}\sum_{j=1}^{n} x_j^2}} \sqrt{\frac{\pi}{2}} \left(\prod_{j=1}^{n} x_j \right) \sum_{j=0}^{n-2} \frac{(2n-4-j)!}{2^{n-2-j}\, j! (n-2-j)! \alpha^{j+2} \left(\sum_{j=1}^{n} x_j^2 \right)^{\frac{2n-3-j}{2}}} \tag{68}$$

Finally, the updated VBM, which represent the underlying random variable X, is given by

$$f\left(M_{w,Hs,U,H}\right)=\frac{M_{w,Hs,U,H}}{\left(\hat{\theta}''\right)^2}e^{\frac{\left(M_{w,Hs,U,H}\right)^2}{2\left(\hat{\theta}''\right)^2}} \qquad \hat{\theta}'', M_{w,Hs,U,H} \geq 0 \tag{69}$$

For large sets of observation, in order to avoid numerical problems (e.g. the likelihood function $L(\theta)$), it is convenient to use an appropriate set of units and consider to use a logarithmic form. Also, it may be recommended to use simulation-based algorithms.

6.3. Illustrative Example

Based on the data provided by Devine (2009), the developed approach is applied to the Joint High-Speed Sealift (JHSS). Since the raw signals include both low- and high-frequency responses, they are filtered by using the Butterworth filter with cutoff frequency of 0.5 Hz for the VBM and 0.4 Hz for the HBM. These cutoff frequencies were estimated by analyzing the Fourier transform of the raw signals. It is noticed that the signals can be split into two regions containing the low and high peak frequencies. Similar results are obtained for the HBM. Moreover, a cleaner signal has been obtained by cutting off the noise for frequencies greater than 5 Hz, that are insignificant for the analysis.

Figure 29 shows the integration of collected observations of VBM through Bayesian updating. Figures 29(a,b) show partial updating considering 1 and 30 observations, respectively. It can be noticed that the weight of the SHM data (extracted peaks) with respect to the prior distribution (Rayleigh) becomes more significant when the set of these data gets larger. The posterior distributions (Rayleigh), governed by the expected value of parameter θ, are evaluated using both close-form solution and simulation-based techniques by using the slice sampling algorithm. The two methods indicate complete agreement; then, by incorporating all extracted peaks, the final updated posterior distributions are obtained, as shown in Fig. 29(c,d) for VBM of signals 1 (number of peaks n_{SHM} = 402) and signal 2 (number of peaks n_{SHM} = 449), respectively. Figure 29(c,d) report also on partial updating, indicating partial updated posteriors in dashed light gray curves. Besides, the high-frequency VBM is used without being updated, because its prior information is insufficient and not specific for any combination of *Hs*, *U*, and *H*.

Once VBM is initially predicted, and after filtering the SHM data, some of the VBMs belonging to the proper operational condition *Hs*, *U*, and *H* of signals are updated accordingly. Figure 30 shows the profiles of the assessed performances (VBM, reliability index, probability of exceedance, and risk), including both initial prediction and updated information (indicated with a light gray shaded region). In detail, Fig. 30 (a) shows the polar representation of the VBM (two different scales are shown), given *Hs* = 9.14 m and *U* = 18 m/s. Figure 30(b) shows the polar profiles of the reliability index associated with the four limit states *LS*1 to *LS*4 for the intact ship (t = 0 years) and for an aged ship (t = 30 years), given *Hs* = 9.14 m and *U* = 18 m/s. Reliability index is lower when corrosion effects are considered for the aged ship case, therefore the associated risk is expected to be higher than the intact ship case. Figure 30(c) shows the profiles of the probability of exceedance associated with the limit states *LSi*, fixing *U* = 18 m/s and *H* =

0°, and reports on the probabilities for the intact ship of being in states *S*1 to *S*5. Figure 30(d) shows the profiles of direct and indirect risks associated with states *S*2 to *S*5 of the intact ship (*S*1 does not generate any consequences). According to the cost analysis, indirect risk is much greater that direct risk. The updated risk is almost negligible when the ship is traveling under this specific Hs = 9.14 m, U = 18 m/s, and $20° \leq H \leq 20°$ combination compared to risk with H = 180°.

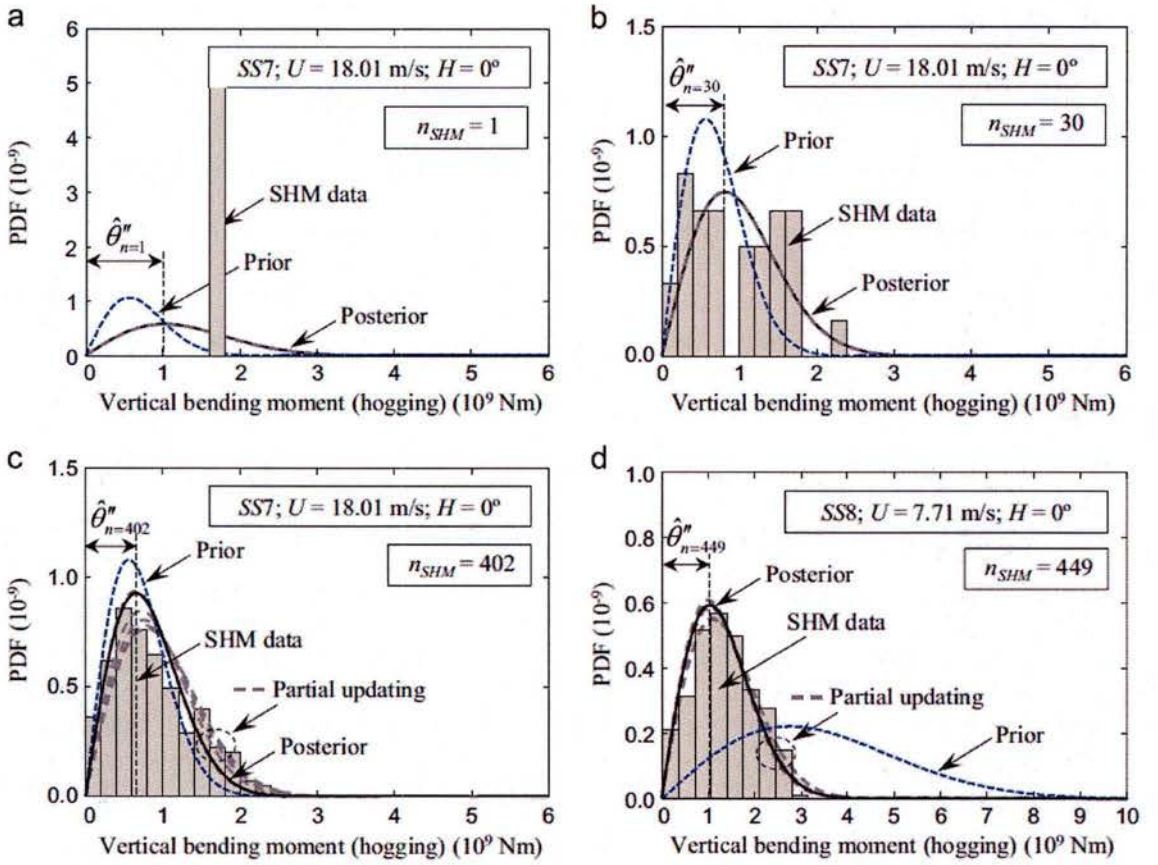

Figure 29 Updating process including prior distributions, SHM histograms, and posterior distributions for the VBMs of (a–c) signal 1 and (d) signal 2, where SS indicates the sea state, S is the ship speed and H is the heading angle. Partial distribution for VBM signal 1 with n_{SHM} = 1 and n_{SHM}=30 are shown in (a) and (b), respectively.

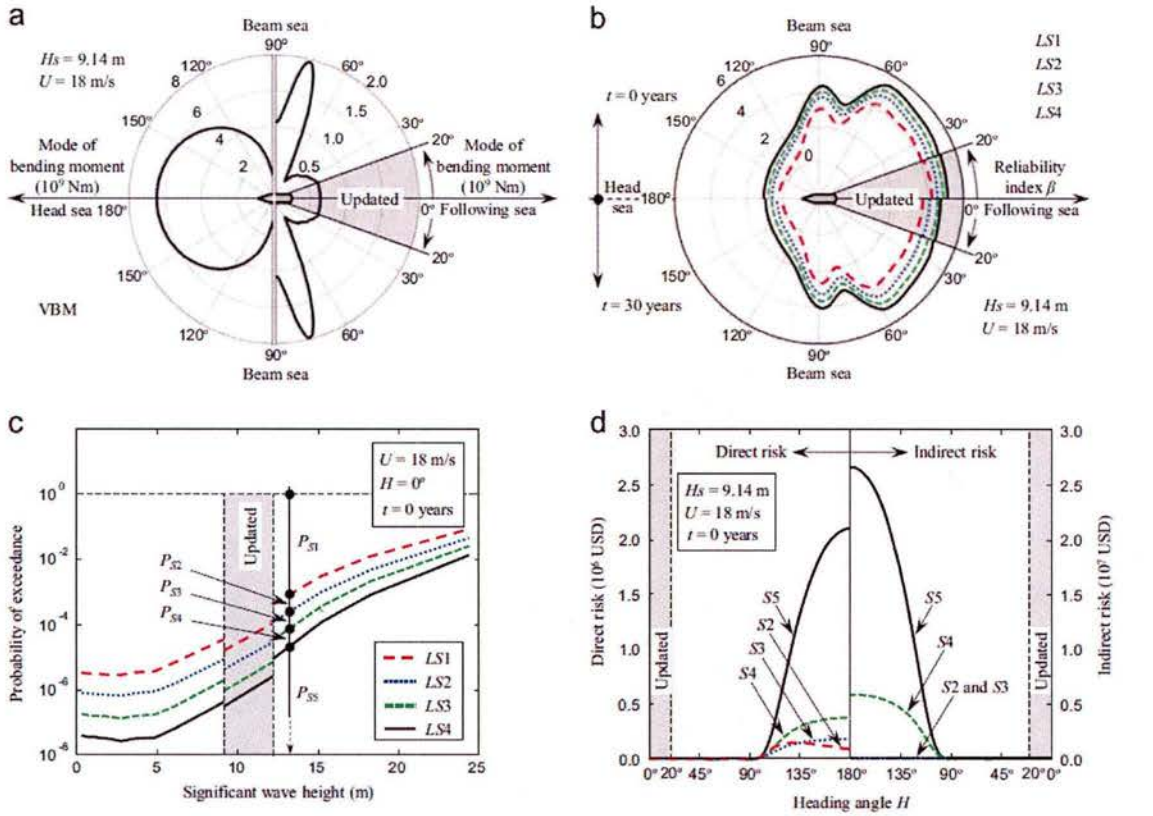

Figure 30 Initially predicted and updated profiles (indicated with a light gray shaded region) of (a) VBM, (b) reliability index (intact ship t=0 years and aged ship t=30 years), (c) probability of exceedance (intact ship t=0), and (d) direct and indirect risk (intact ship t=0).

After obtaining updated parameters, an optimization problem is formulated and solved using genetic algorithms. Figure 31 shows Pareto fronts obtained by solving optimization problem considering SHM. Three objectives (i.e., estimated time of arrival, mean total risk, and fuel cost) are simultaneously minimized. The solutions to the problems are 3D Pareto fronts as reported in Fig. 31(a). Generally, it can be noticed that higher fuel cost is generally associated with low risk levels because fuel consumption is related to the ship speed and the encountered sea conditions, therefore when longer patterns are chosen, risk decreases, whereas fuel cost increases. Although the latter seems always true, the opposite does not occur. In fact, low fuel cost may be associated with high or low risk levels, depending on the followed route. Moreover, solutions with high ETA are generally associated with low risk, due to longer routes in order to avoid dangerous situations. Four solutions are extrapolated from each Pareto set I, J, K, and L, reported in Fig. 31(b,c,d,e,f,g), respectively. Accordingly, the route profiles with respect to total risk (USD), fuel cost (USD), reliability index, the value of the *y*-axis (km), ship speed (m/s), and cumulative time from departure (h) are reported. Instead of presenting the route pattern through sea maps, *y*-axis coordinates are provided (Fig. 31(e)) in this case. Risk is high and reliability index down crosses critical levels when route E is selected, since it is the shortest and fastest path. Although the

speed profile of route H is relatively low, and route H has the lowest fuel cost among the selected routes, its risk profile is not as low, because its path goes through the storm.

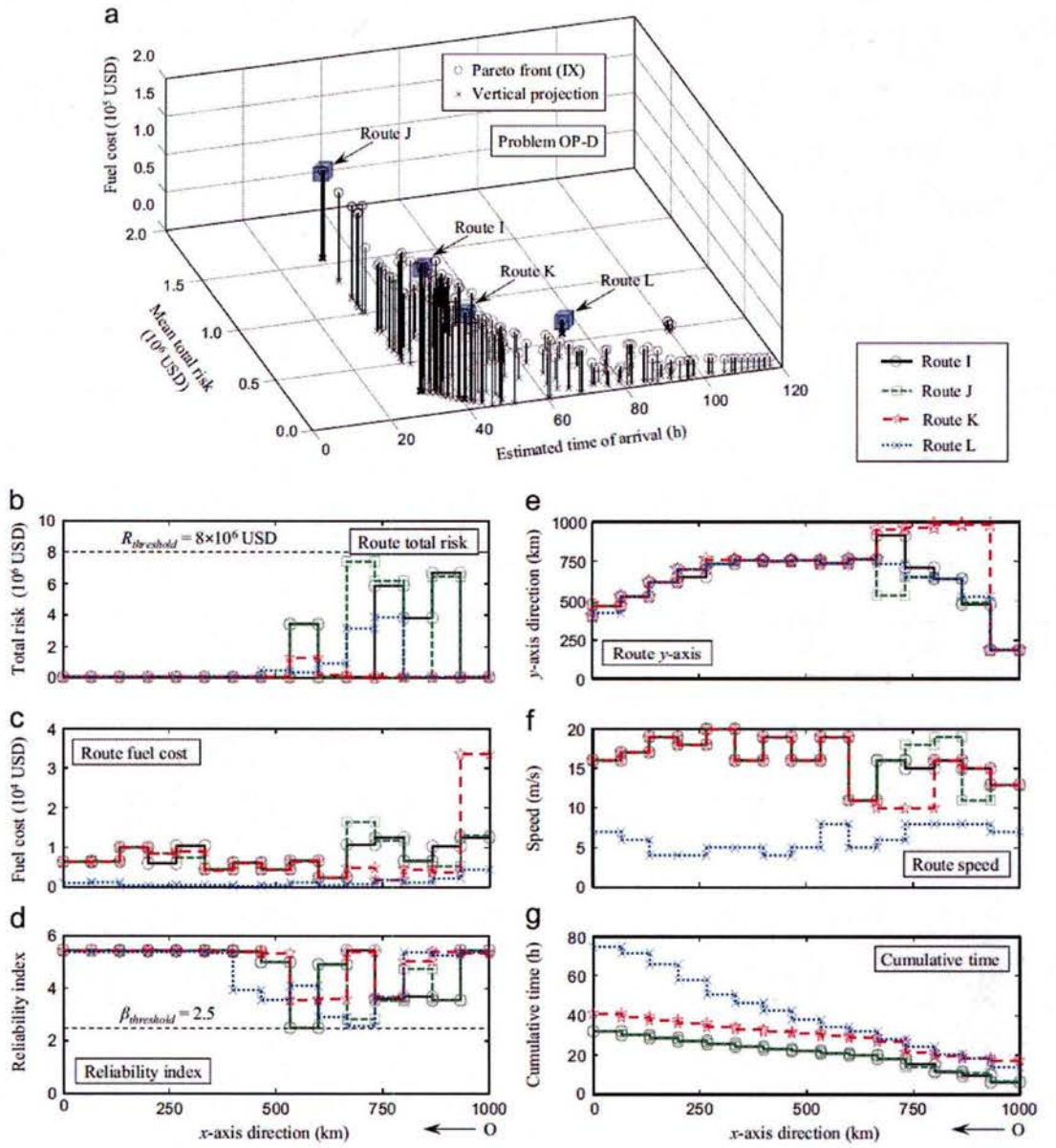

Figure 31 Pareto fronts obtained by solving the tri-objective optimization problem and assuming $\beta_{threshold}$ and $R_{threshold}$ equal to 2.5 and $8x10^6$ USD, respectively. Four optimal short range routes denoted routes I, J, K, and L are selected. Profiles of the four solutions, reporting on (b) route total risk (USD), (c) fuel cost (USD), (d) route reliability index associated with ultimate failure (LS4), (e) route y-axis value (km), (f) ship speed (m/s), and cumulative time from departure (h).

6.4. Conclusions

This investigation presented and approach for the integration of SHM data, through Bayesian updating, into risk assessment of ship hulls. A novel closed-form solution for short term statistics based on Rayleigh prior distribution is developed and compared against a simulation-based technique. Then, as an application an approach for real-time optimal routing of ships has been presented. Three-objective optimization problems are solved by minimizing estimated time of arrival (ETA), total risk, and fuel costs. The results are shown in the form of Pareto-optimal sets. Mission profiles including total risk, reliability index, fuel cost, ship path, ship speed, and cumulative time from departure are obtained for a NAVY's JHSS. The information obtained from SHM and different sea weather maps are integrated within the developed optimization framework.

The following conclusions are drawn:

- It is found that optimizing three objectives, including the minimization of ETA, total risk, and fuel cost provides a comprehensive set of optimal solutions. Although some solutions are trivial (e.g. the shortest path), some others need to be further analyzed by decision makers to understand their values. It is found that a higher fuel cost is generally associated with low risk, whereas the opposite is not always true. Moreover, solutions with high ETA are typically associated with low risk, due to longer routes necessary to avoid dangerous situations. Generally, it is also found that having different sea maps available allows the decision maker to select routes that potentially reduce risk; in fact the associated Pareto fronts, when WP is considered, have lower risk than those based on the current sea map only. The selected solutions clearly show how routes correlate with the identified sea/weather system, adapting well through the two systems.
- The importance of considering constraints within the investigated optimization problems is demonstrated. These constraints limit ship operations so that they remain within specific boundaries, allowing slowest paths and reduced traveling speeds.
- The developed approach is flexible, and can update the optimal solutions by including additional data about specific fuel consumption and further SHM data accounting for different combinations of Hs, U, and H.

The presented optimization procedure focuses on the safety of the primary structure of ships, excluding those traveling situations that mostly affect ship stability, which can be added to the problem, by means of serviceability limit states. Moreover, the proposed approach provides additional insights that, although out of the scope of this study, are worth mentioning and can be the subject of future studies, including:

- Considerations regarding the benefit induced by the installation of permanent systems for data collections and SHM.
- The possibility of accounting for probabilistic weather prediction, therefore studying a range of routes associated with different probability of weather/sea occurrence.

GENERAL CONCLUSIONS

This report summarizes the research work conducted during the time interval 12-1-2011 to 9-30-2016. Methodologies developed for predicting time-dependent performance of ships considering sudden and progressive damage under different operational conditions are presented. A computational framework for quantifying the structural reliability and redundancy is developed. Additionally, the effect of integrating SHM information on reliability and redundancy evaluation using advanced updating techniques is investigated. An approach for integrating SHM data to evaluate the reliability of aluminum ship details with respect to fatigue is proposed. Methodologies for the optimal planning of SHM and inspection activities and enhanced near real-time risk-based decision making are also investigated. Application of SHM and updating techniques to support near-real time decision making with respect to ship routing are presented. Based on the results of this investigation, the following conclusions can be drawn:

1. Some operational conditions lead to significant drop of redundancy. When the structural performance reaches a set threshold (warning situation), operational conditions must be modified according to the residual structural safety by reducing the forward speed, or by changing the heading angle in order to improve the structural performance.
2. Integration of the SHM data can significantly reduce the uncertainty in a distribution parameter so that the updated performance indicators are closer to their true values. For the analyzed JHSS, the distribution types of the parameters α of three stations remain the same after updating while the mean values and standard deviations of α change. Therefore, the reliability and redundancy indexes associated with investigated vessel at the heading angle 0° changed although the differences before and after updating were slight.
3. Several combinations of speeds, sea states, and wave headings have a significant effect on fatigue damage accumulation. These operational conditions should be identified and they should be avoided to prevent the accelerated damage to the ship structure. SHM data can be analyzed to identify these operational conditions and assist in quantifying the damage resulting from operation in such conditions.
4. Risk has been proven to be an indicator suitable for measuring the structural performance of ship structures. Especially, when combined with reliability index, it provides solid baseline information that can be used for different management applications, including optimal ship routing.
5. SHM provides additional data that are used to update the prediction of structural performance. A novel closed-form solution, based on the accepted assumption that the peak responses follow the Rayleigh distribution, is developed in this investigation. The profiles of load effects in terms of VBM and HBM, reliability index, and risk have been successfully updated by using test data of a scaled ship model of the JHSS.

REFERENCES

ABS, (1995). Guide for Assessing Hull-Girder Residual Strength for Tankers. American Bureau of Shipping.

Akpan, U. O., Koko, T. S., Ayyub, B. and Dunbar, T. E. (2002). Risk assessment of aging ship hull structures in the presence of corrosion and fatigue. *Marine Structures*, Elsevier, 15(3), 211-231.

Ang, A. H.-S. and Tang, W. H. (2007). Probability concepts in engineering. Emphasis on applications to civil and environmental engineering. 2nd ed. *New York: Wiley & Sons.*

Ayyub, B. M., Assakkaf, I., Atua, K., Engle, A., Hess, P. E., Karaszewski, Z., Kihl, D., Melton, W., Sielski, R. A., Sieve, M., Waldman, J. and White, G. J. (1998). *Reliability-based Design of Ship Structures: Current Practice and Emerging Technologies*. Research Report to the US Coast Guard, SNAME, T&R Report R-53.

Ayyub, B. M., Assakkaf, I. A. and Atua, K. I. (2000). Reliability-based load and resistance factor design (LRFD) of hull girders for surface ships. *Naval Engineers Journal*, ASNE, 112(4), 279-296.

Ayyub, B. M., Akpan, U. O., Rushton, P. A. and Koko, T. S. (2002). *Risk-Informed Inspection of Marine Vessels*. Ship Structure Committee: SSC-421.

Bertram, V., Söding, H. and Graf, K. (2006). PDSTRIP – A strip method for ship and yacht seakeeping. 9th Numerical Towing Tank Symposium, 1-3 October 2006, Le Croisic, France.

Benjamin, J. R. and Cornell, C. A. (1970). Probability, Statistics, and Decision for Civil Engineers. *New York: McGraw-Hill Book Company.*

Brady T.F., 2004a. *HSV-2 Swift instrumentation and technical trials plan.* NSWCCD-65-TR-2004/18, Naval Surface Warfare Center, Carderock Division, West Bethesda, MD.

Brady T.F., 2004b. *Wave impact loading response measurement and analysis for HSV-2 from JLOTS and blue game rough water trials.* NSWCCD-65-TR- 2004/32, Naval Surface Warfare Center, Carderock Division, West Bethesda, MD.

Bucher, C. G. and Bourgund, U. (1990). A Fast and Efficient Response Surface Approach for Structural Reliability Problems. *Structural Safety*, Elsevier, 7, 57-66.

Collette, M. and Incecik, A., (2006). An approach for reliability-based fatigue design of welded joints in aluminum high-speed vessels. *Journal of Ship Research*, 50(3): 85-98.

Decò, A. and Frangopol, D. M. (2013). Risk-informed optimal routing of ships considering different damage scenarios and operational conditions, *Reliability Engineering & System Safety*, 119, 126-140.

Decò, A. and Frangopol, D. M. (2015). Real-time risk of ship structures integrating structural health monitoring data: Application to multi-objective optimal ship routing, *Ocean Engineering*, 96(1), 312-329.

Decò, A., Frangopol, D. M. and Okasha, N. M. (2011). Time-variant redundancy of ship structures. *Journal of Ship Research*, SNAME, 55(3), 208-219.

Decò, A., Frangopol, D. M. and Zhu, B. (2012). Reliability and Redundancy Assessment of Ships under Different Operational Conditions, *Engineering Structures*, Elsevier, 42, 457-471.

Devine, E. A. (2009). An overview of the recently-completed JHSS monohull and trimaran structural seaways loads test program. Naval Surface Warfare Center, Carderock Division (NSWCCD), PowerPoint Briefing, 30 October, 2009.

Dinovitzer, A. (2003). *Life Expectancy Assessment of Ship Structures*. Ship Structure Committee: SSC-427.

Estes, A. C. and Frangopol D. M. (1998). RELSYS: A Computer Program for Structural System Reliability Analysis. *Structure Engineering and Mechanics*, Techno Press, 6(8), 901-19.

Faltinsen, O. M. (1990). *Sea Loads on Ships and Offshore Structures*. Cambridge University Press, Cambridge, UK, 328p.

Frangopol, D. M. (2011). Life-cycle performance, management, and optimization of structural systems under uncertainty: accomplishments and challenges. *Structure and Infrastructure Engineering*, 7(6), 389-413.

Frangopol, D. M. and Curley, J. P. (1987). Effects of Damage and Redundancy on Structural Reliability. *Journal of Structural Engineering*, ASCE, 113(7), 1533-1549.

Frangopol, D. M., Bocchini, P., Decò, A., Kim, S., Kwon, K., Okasha, N. M. and Saydam, D. (2012). Integrated life-cycle framework for maintenance, monitoring, and reliability of naval ship structures. *Naval Engineers Journal*, 124(1), 89-99.

Frangopol, D. M., Bocchini, P., Decò, A., Kim, S., Kwon, K., Okasha, N. M., Saydam, D. and Salvino, L. W. (2011). Life-cycle ship reliability assessment, damage detection, and optimization. Proceeding of the Eleventh International Conference on Fast Sea Transportation FAST 2011 (T. J. Peltzer ed.), ASNE, Honolulu, HI, September 26-29, 2011, pp. 555-560.

Frangopol, D. M., Bocchini, P., Decò, A., Kim, S., Kwon, K., Okasha, N. M., Saydam, D. (2012). Integrated Life-Cycle Framework for Maintenance, Monitoring, and Reliability of Naval Ship Structures. *Naval Engineers Journal*, 124(1), 89-99.

FREE!ship (2006). *FREE!ship manual - Version 2.6*. Website: www.freeship.org (accessed October 2011).

Glen, I. F., Paterson, R. B. and Luznik, L. (1999). *Sea Operational Profiles for Structural Reliability Assessment*. Ship Structure Committee: SSC-406.

Gordo, J. M. and Guedes Soares, C. (1996). Approximate Methods to Evaluate the Hull Girder Collapse Strength. *Marine Structures*, Elsevier, 9(3), 449-470.

Gordo, J. M. and Guedes Soares, C. (1997). Interaction Equation for the Collapse of Tankers and Containership under Combined Bending Moments. *Journal of Ship Research*, SNAME, 41(3), 230-240.

Guedes Soares, C. (1992). Combination of primary load effects in ship structures. *Probabilistic Engineering Mechanics*, 7(2), 103-111.

Guedes Soares, C. and Teixeira, A. P. (2000). Structural Reliability of two Bulk Carrier Designs. *Marine Structures*, Elsevier, 13(2), 107-128.

Guedes Soares, C. and Garbatov, Y. (1999). Reliability of maintained ship hulls subjected to corrosion and fatigue under combined loading. *Journal of Constructional Steel Research*, 52(1), 93-115.

Hughes, O. F. (1983). *Ship Structural Design: A Rationally-Based, Computer-Aided, Optimization Approach*. Wiley and Sons, New York, 582p.

Hussein, A. W. and Guedes Soares, C. (2009). Reliability and residual strength of double hull tankers designed according to the new IACS common structural rules. *Ocean Engineering*, 36(17-18), 1446-1459.

IACS (2008). *Common Structural Rules for Double Hull Oil Tankers*. International Association of Classification Societies (IACS), London, UK. Website: http://www.iacs.org.uk.

IMO (1997). MSC/Circ. 829 and MEPC/Circ. 335. Interim Guidelines for the Application of Formal Safety Assessment (FSA) to the IMO Rule-Making Process. International Maritime Organization (IMO), London, UK.

Khan, I.A., and Das, P.K., (2008). Reliability analysis of intact and damaged ships considering combined vertical and horizontal bending moments. *Ships and Offshore Structures*, 8(3), 371–384.

Korvin-Kroukowski, B. V. and Jacobs, W. R. (1957). Pitching and heaving motions of a ship in regular waves. *Transactions*, SNAME, 65, 590-632.

Liu P.L., Lin H.Z., and Der Kiureghian A., 1989. *CalREL User Manual*, Department of Civil Engineering. University of California, Berkeley, CA.

Lua, J. and Hess, P. E. (2003). Hybrid reliability predictions of single and advanced double-hull ship structures. *Journal of Ship Research*, SNAME, 47(2), 155-176.

Lua, J. and Hess, P. E. (2006). First-failure-based reliability assessment and sensitivity analysis of a naval vessel under hogging. *Journal of Ship Research*, SNAME, 50(2), 158-170.

Luís, R. M., Teixeira, A. P. and Guedes Soares, C. (2009). Longitudinal strength reliability of a tanker hull accidentally grounded. *Structural Safety*, 31(3), 224-233.

Mansour, A. E. and Thayamballi, A. (1994). *Probability based Ship Design; Loads and Load Combinations*, Ship Structure Committee: SSC-373.

Mansour, A. E. (1997). *Assessment of Reliability of Ship Structures*. Ship Structure Committee: SSC-398.

Mansour, A. E. and Hovem, L. (1994). Probability based ship structural safety analysis. *Journal of Ship Research*, SNAME, 38(4), 329-339.

Michel, W. H. (1999). Sea spectra revisited. *Marine Technology*, SNAME, 36(4), 211-227.

Miner M. A., 1945. Cumulative damage in fatigue. *Journal of Applied Mechanics*, 12(3): 159-164.

Miroyannis, A. (2006). *Estimation of Ship Construction Costs*. B.S. Thesis, Department of Mechanical Engineering, Massachusetts Institute of Technology, Boston, MA.

Okasha, N. M. and Frangopol, D. M. (2010). Efficient method based on optimization and simulation for the probabilistic strength computation of the ship hull. *Journal of Ship Research*, SNAME, 54(4), 1-13.

Okasha, N. M., Frangopol, D. M., Decò, A. (2010). Integration of structural health monitoring in life-cycle performance assessment of ship structures under uncertainty. *Marine Structures*, 23(3), 303-321.

Okasha, N. M., Frangopol, D. M., Saydam, D., Salvino, L. M. (2011). Reliability analysis and damage detection in high-speed naval craft based on structural health monitoring data. *Structural Health Monitoring*, 10(4), 361-379.

Paik, J. K., Thayamballi, A. K. and Che, J. S. (1996). Ultimate Strength of Ship Hulls under Combined Vertical Bending, Horizontal Bending, and Shearing Forces. *Transactions of SNAME*, 104, 31-59.

Paik, J. K. and Frieze, P. A. (2001). Ship structural safety and reliability. *Progress in Structural Engineering and Materials*, 3(2), 198-210.

Paik, J. K., Kim, S. K. and Lee, S. K. (1998). Probabilistic corrosion rate estimation model for longitudinal strength members of bulk carriers. *Ocean Engineering*, 25(10), 837-860.

Palladino, F., Bouscasse, B., Lugni, C. and Bertram, V. (2006). Validation of ship motion functions of PDSTRIP for some standard test cases. 9th Numerical Towing Tank Symposium, 1-3 October 2006, Le Croisic, France.

Papoulis, A. (1984). *Probability, Random Variables, and Stochastic Processes*. 2nd ed, McGraw-Hill, New York, 576p.

PDSTRIP (2006). *Program PDSTRIP: Public Domain Strip Method - User Manual*. Website: http://sourceforge.net/projects/pdstrip (accessed October 2011).

Resolute Weather (2011). *Pierson-Moskowitz Sea Spectrum*. Website: http://www.eustis.army.mil/weather (accessed October 2011).

Saydam, D., and Frangopol, D. M., (2013). Performance assessment of damaged ship hulls. *Ocean Engineering*, 68, 65-76.

The MathWorks (2009). *Statistics ToolboxTM 7 User's Guide*. The MathWork, Inc., 1749p.

Wang, G., Chen, Y., Zhang, H., and Peng, H.,(2002a). Longitudinal strength of ships with accidental damages. *Marine Structures*, 15, 119–138.

Wang, G., Spencer, J., Chen,Y.J., and (2002b). Assessment of ship's performance in accidents. *Marine Structures*, 15, 313–333.

Zhu, B. and Frangopol, D. M., (2013). Incorporation of SHM data on load effects in the reliability and redundancy assessment of ship cross-sections using Bayesian updating. *Structural Health Monitoring*, 12(4), 377-392.